

大别山千鹅冲钼矿区花岗岩的 SHRIMP 锆石 U-Pb 年龄、Hf 同位素组成及微量元素特征*

高阳¹ 叶会寿^{1**} 李永峰² 罗正传² 李法岭³ 熊必康⁴ 孟芳⁴

GAO Yang¹, YE HuiShou^{1**}, LI YongFeng², LUO ZhengZhuan², LI FaLing³, XIONG BiKang⁴ and MENG Fang⁴

1. 中国地质科学院矿产资源研究所, 国土资源部成矿作用与资源评价重点实验室, 北京 100037

2. 河南省有色金属地质矿产局, 郑州 450016

3. 河南省地矿局第三地质调查队, 信阳 464000

4. 中国地质大学, 北京 100083

1. MLR Key Laboratory of Metallogeny and Mineral Assessment, Institute of Mineral Resources, Chinese Academy of Geological Sciences, Beijing 100037, China

2. Henan Provincial Non-ferrous Metals Geological and Mineral Resources Bureau, Zhengzhou 450016, China

3. No. 3 Geological Survey, Henan Bureau of Geology and Mineral Resources, Xinyang 464000, China

4. China University of Geosciences, Beijing 100083, China

2013-09-02 收稿, 2013-12-07 改回.

Gao Y, Ye HS, Li YF, Luo ZZ, Li FL, Xiong BK and Meng F. 2014. SHRIMP zircon U-Pb ages, Hf isotopic compositions and trace elements characteristics of the granites from the Qian'echong Mo deposit, Dabie Orogen. *Acta Petrologica Sinica*, 30(1):49–63

Abstract The Qian'echong porphyry Mo deposit is located in the Dabie area, the eastern part of the East Qinling-Dabie molybdenum belt. The molybdenum mineralization mainly hosted by the Devonian Nanwan Formation in the external contact zone, with minor by the Qian'echong concealed stock, which consists of monzogranite and granite porphyry. Sensitive high-resolution ion microprobe (SHRIMP) zircon U-Pb dating constrains the crystallization of the monzogranite and granite porphyry at 130 ± 2 Ma and 129 ± 2 Ma, respectively. They are quite in accordance with each other within errors, indicating the Early Cretaceous magmatism. According to zircon Hf isotope analyses, the $\varepsilon_{\text{Hf}}(t)$ values of monzogranite and granite porphyry are $-24.5 \sim -2.7$ and $-19.8 \sim -11.2$, respectively. Both the monzogranite and the granite porphyry have large ranges of $\varepsilon_{\text{Hf}}(t)$ values, indicating that they mainly derived from the partial melting of ancient crust, with minor juvenile components. The calculated $t_{2\text{DM}}$ values from Hf isotopes and Paleoproterozoic inherited zircon suggest that Paleoproterozoic-Archean basement rocks have been involved in the source rocks of these granites. The zircons from the monzogranite and granite porphyry have average $\text{Ce}^{4+}/\text{Ce}^{3+}$ ratios of 287.4 and 55.9, respectively, suggesting that the monzogranite were in higher oxygen fugacity than the granite porphyry, however, the Mo mineralization is more likely related to the later-formed granite porphyry. The Qian'echong Mo deposit formed at an Early Cretaceous lithospheric extensional setting in the Dabie orogen. The delamination caused asthenosphere upwelling and mantle-crust interaction, which probably provided ore-forming material of Qian'echong Mo deposit.

Key words SHRIMP zircon U-Pb age; Hf isotope; Qian'echong Mo deposit; Dabie

摘要 千鹅冲斑岩型钼矿床位于东秦岭-大别钼矿带东部的大别山地区。矿体主要赋存于千鹅冲隐伏花岗岩体上部(外接触带)的南湾组片岩中,少量产于花岗岩体内。矿体下部的隐伏岩体中主要见有二长花岗岩和花岗斑岩。SHRIMP 锆石 U-Pb 定年表明,二长花岗岩和花岗斑岩的侵位年龄分别为 130 ± 2 Ma (MSWD = 1.4) 和 129 ± 2 Ma (MSWD = 1.9),二者年龄一致,说明隐伏岩体形成于早白垩世。锆石 Hf 同位素分析结果表明,千鹅冲钼矿中二长花岗岩和花岗斑岩的 $\varepsilon_{\text{Hf}}(t)$ 值分别变化于

* 本文受地质调查项目(1212011220869)、国家自然科学基金项目(41272104)和国家科技支撑计划项目(2011BAB04B06)联合资助。

第一作者简介:高阳,男,1984年生,博士生,矿床学专业,E-mail: gy.36@163.com

** 通讯作者:叶会寿,男,1964年生,研究员,矿床学专业,E-mail: yehuishou@163.com

-24.5 ~ -2.7 和 -19.8 ~ -11.2 之间,变化范围较大,说明它们主要来源于古老地壳的部分熔融,也有年轻组分的参与。两阶段模式年龄(t_{DM2})和古元古代的继承锆石指示这些花岗岩的原岩中含有古元古代-太古代的基底岩石。二长花岗岩和花岗斑岩中的锆石的 Ce^{4+}/Ce^{3+} 比值平均值分别为 287.4 和 55.9,说明形成二长花岗岩的岩浆具有更高的氧逸度,但钼成矿与形成较晚的花岗斑岩具有更紧密的成因联系。千鹅冲钼矿形成于大别造山带早白垩世的伸展构造体制下,造山带下地壳折沉作用造成的软流圈上涌和壳幔相互作用可能为钼矿的形成提供了成矿物质。

关键词 SHRIMP 锆石 U-Pb 年龄;Hf 同位素;千鹅冲钼矿;大别山

中图法分类号 P588.121; P597.3

1 引言

千鹅冲钼矿床位于秦岭-大别造山带东部的大别山地区,是东秦岭-大别钼矿带近年来发现的一处超大型钼矿床,已探明钼资源量 60 万吨,平均品位 0.08% (李法岭, 2011; Mao *et al.*, 2011a)。2006 年开始,河南省第三地质调查队在千鹅冲地区实现了找矿突破,发现了矿区南部南湾组片岩中的千鹅冲隐伏岩体及其上部的隐伏矿体,最终确定其为超大型规模,并且是大别山地区发现的第一个超大型钼矿床。千鹅冲钼矿床的发现不仅结束了大别山地区无超大型矿床的历史,同时对区域上找矿勘探也具有十分重要的指导意义。

自千鹅冲钼矿发现以后,多位学者就其成矿成岩时代、成矿流体特征等进行了研究。研究结果表明,千鹅冲钼矿辉钼矿 Re-Os 同位素年龄为 128 ± 8 Ma (李法岭, 2011; 杨梅珍等, 2010),成矿作用发生在早白垩世;成矿流体为高温、高盐度、贫子晶、富 CO_2 的流体系统 (Yang *et al.*, 2013)。钻探工程揭露矿体下部存在隐伏岩体,并且与矿体具有紧密的空间关系,所以对千鹅冲隐伏岩体进行年代学研究对于揭示成岩成矿关系及成矿机制都具有重要意义。本次研究对矿体下部隐伏的二长花岗岩和花岗斑岩进行了 SHRIMP 锆石 U-Pb 同位素定年,从而精确厘定了千鹅冲隐伏岩体的形成时代,并通过锆石原位 Hf 同位素及锆石微量元素分析,浅析千鹅冲隐伏岩体的成因、构造背景及与成矿的关系,同时为深入研究大别山地区白垩纪钼成矿作用与区域大规模花岗岩岩浆作用的关系提供了重要依据。

2 区域地质背景

大别造山带是秦岭-大别-苏鲁造山带的组成部分,形成于三叠纪华北与华南两板块的碰撞拼合 (图 1) (张国伟等, 2001; Hacker *et al.*, 1998; Li *et al.*, 2001; Ratschbacher *et al.*, 2003)。大别造山带西起河南桐柏山,向西以南阳盆地界与秦岭造山带相望,东侧为郟城-庐江断裂,此断裂使大别造山带和苏鲁造山带之间位移约 500km。大别造山带南北边界分别为襄樊-广济断裂和栾川-明港-固始断裂。

大别造山带以商城-麻城断裂为界可分为东大别和西大别两部分。东大别从北到南分别以晓天-磨子潭断裂 (XMF)、五河-水吼断裂 (WSF) 和太湖-马庙断裂 (TMF) 为边

界可划分出 4 个岩石-构造单元 (Li *et al.*, 2001; 向必伟, 2009): (1) 北淮阳构造带,主要包括一套在华南板块向北华板块俯冲时刮削下来所形成的低级变质地体 (Zheng *et al.*, 2005),变质岩原岩具有 700 ~ 800Ma 的锆石 U-Pb 年龄 (Hacker *et al.*, 2000; Chen *et al.*, 2003); (2) 北大别杂岩带,主要由大规模白垩纪花岗岩及少量镁铁-超镁铁质侵入岩、新元古代 TTG 片麻岩和角闪岩、三叠纪榴辉岩、少量变质沉积岩和麻粒岩以及少量橄辉岩组成 (Hacker *et al.*, 2000; Bryant *et al.*, 2004; Liu *et al.*, 2005; Xu *et al.*, 2000; Zheng *et al.*, 2003); (3) 南大别高压-超高压变质带,以产出含柯石英和石榴榴辉岩为特征 (Wang *et al.*, 1989),主要包括榴辉岩、含石榴石橄辉岩、硬玉石英岩、大理岩、石榴石-二云母片岩及片麻岩 (Hacker *et al.*, 1998, 2000; Xu *et al.*, 2003); (4) 宿松杂岩带,主要包含中-新元古代变质沉积岩和变质火山岩以及震旦纪大理岩 (You *et al.*, 1996)。西大别具有与东大别相似的岩石-构造单元组成,不同的是西大别缺少与“北大别杂岩带”相对应的构造单元。

大别山地区发育大量中生代岩浆岩,其显著特点是全部形成于早白垩世,主要包括大量中酸性侵入岩及少量镁铁-超镁铁质岩和火山岩 (Fan *et al.*, 2004; He *et al.*, 2011, 2013; Huang *et al.*, 2008; Wang *et al.*, 2007; Zhao *et al.*, 2005)。早白垩世花岗岩类侵位时间为 117 ~ 143Ma (He *et al.*, 2011; Wang *et al.*, 2007),可分为两期,早期岩体 (130 ~ 143Ma) 通常具有高的 Sr/Y 和 La/Yb 比值,而晚期岩体则通常不具备这一特征 (Wang *et al.*, 2007; Xu *et al.*, 2007)。火山岩主要分布在北淮阳构造带内,主要包括玄武质粗安岩、粗安岩及粗面岩等 (Fan *et al.*, 2004)。镁铁-超镁铁质侵入岩主要发育在北大别杂岩带内,时代为 123 ~ 130Ma,主要包括辉石岩、角闪石岩、辉长岩等 (Dai *et al.*, 2011; Huang *et al.*, 2007; Wang *et al.*, 2005; Zhao *et al.*, 2005)。

目前在大别山地区发现的斑岩型钼矿床主要分布在中西部的北淮阳构造带及临近地区 (图 1)。斑岩钼矿与早白垩世中酸性小斑岩体具有紧密的时空关系,其产出明显受网格状断裂构造的控制。

3 矿床地质特征

千鹅冲钼矿床位于西大别北淮阳构造带内,区域性桐柏-商城断裂带北侧 (图 1)。矿区出露地层比较简单,绝大部

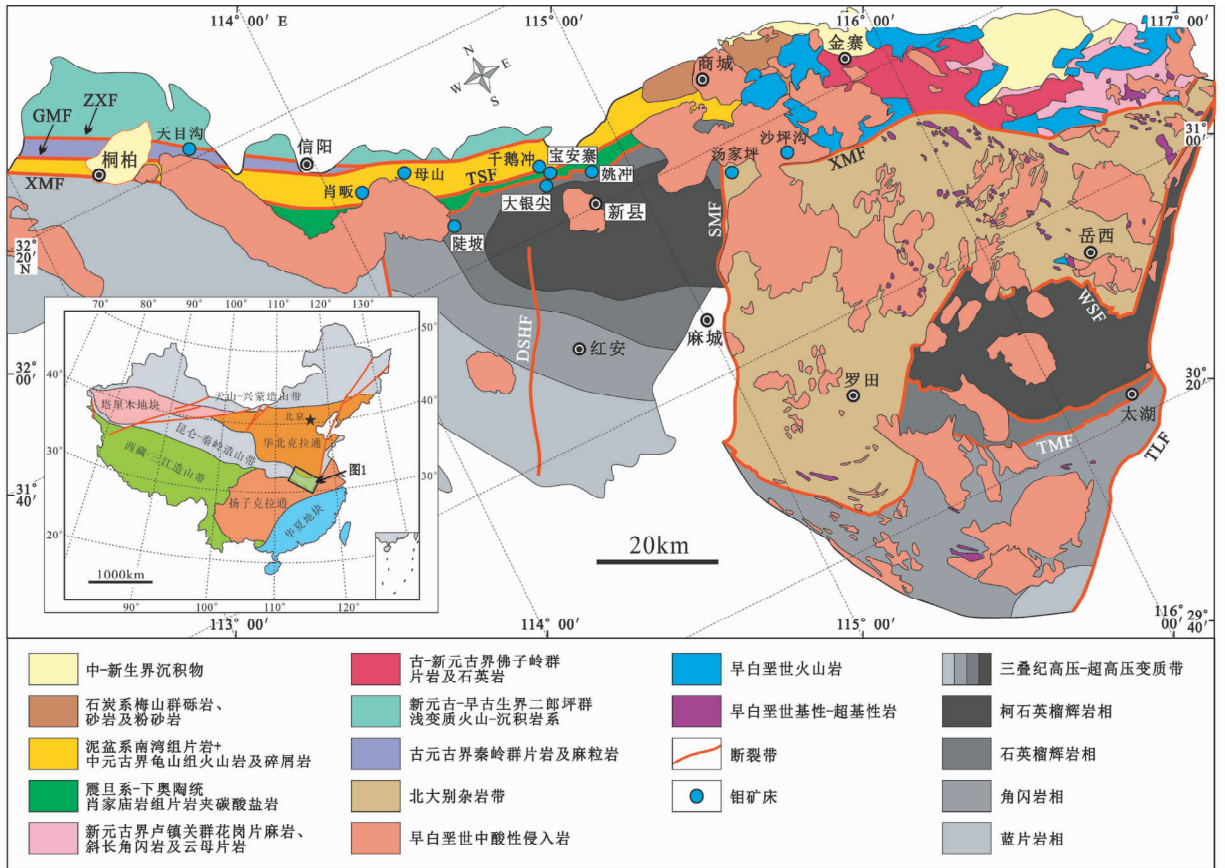


图1 桐柏-大别山地区地质图(据 Ratschbacher *et al.*, 2003 修改)

白垩纪花岗岩及镁铁-超镁铁质岩引自 Ratschbacher *et al.*, 2003; He *et al.*, 2011; Zhao *et al.*, 2005. ZXF, GMF, XMF, TSF, DSHF, SMF, WSF, TMF and TLF 分别代表朱阳关-夏馆断裂、龟山-梅山断裂、晓天-磨子潭断裂、桐柏-商城断裂、陡山河断裂、商城-麻城断裂、五河-水吼断裂、太湖-马庙断裂及郟城-庐江断裂

Fig. 1 Generalized geological map of the Tongbai-Dabie area in East China (modified after Ratschbacher *et al.*, 2003)

Cretaceous granites and mafic-ultramafic intrusive rocks are from Ratschbacher *et al.*, 2003; He *et al.*, 2011; Zhao *et al.*, 2005. ZXF, GMF, XMF, TSF, DSHF, SMF, WSF, TMF and TLF represent the Zhuyanguan-Xiaguan Fault, the Guishan-Meishan Fault, the Xiaotian-Mozitan Fault, the Tongbai-Shangcheng Fault, the Doushanhe Fault, the Shangcheng-Macheng Fault, the Wuhe-Shuihou Fault, the Taihu-Mamiao Fault and Tancheng-Lujiang Fault, respectively

分为泥盆系南湾组 (Dn) 浅变质云母石英片岩系, 另外在矿区西南部边界分布少量震旦系-下奥陶统肖家庙岩组 (Z-O₁x³) 地层以及沟谷中出露的第四系(图2)。区内地层走向北西西, 与区域构造线一致。肖家庙岩组与南湾组以桐-商韧性剪切带为界, 呈构造接触, 构造带以南为肖家庙岩组地层, 以北为南湾组地层。

矿区内无大的褶皱构造, 构造主要为断裂构造。断裂构造分为韧性断裂和脆性断裂。韧性断裂为区域性桐(柏)-商(城)韧性剪切带的一部分, 出露于矿区南部, 为肖家庙岩组与南湾组地层的分界(图2), 韧性剪切带内的构造岩以云英质构造片岩为主, 次为长英质变晶糜棱岩。脆性断裂是矿区内的主要构造形态, 主要发育在矿区中部南湾组地层中, 主要为北西西向和近南北向两组。地表沿断裂分布一系列构造蚀变岩带, 带内岩石发生较强硅化、钾长石化、碳酸盐化及

褐铁矿化, 部分地段发现钼、铜、铅、银矿化。

千鹅冲矿区地表无大岩体出露, 经钻探验证, 在矿区中南部存在隐伏岩体(图2b), 钻孔揭露其顶部标高为-512.71 ~ -751.29m, 岩体呈起伏状与围岩侵入接触, 局部有震碎现象。钻孔控制隐伏岩体平面投影面积约0.262km²。该岩体为矿区钼矿的成矿母岩, 其与围岩接触带可见强弱不等的蚀变, 类型主要有硅化、钾长石化、绢云母化和黄铁矿化, 并伴生钼矿化, 但矿化强度弱于上部围岩。岩体主要由花岗斑岩和二长花岗岩组成, 钻孔中揭露的花岗斑岩含量远多于二长花岗岩, 二长花岗岩只在局部可见。除此之外, 区内燕山晚期中酸性小型脉岩较发育, 按岩石类型可分为闪长玢岩脉、煌斑岩脉、石英斑岩脉和花岗斑岩脉。

除少量矿体产于隐伏岩体内接触带, 绝大部分矿体产于南湾组片岩中。赋矿岩石主要为绿帘黑云石英片岩、绿帘黑

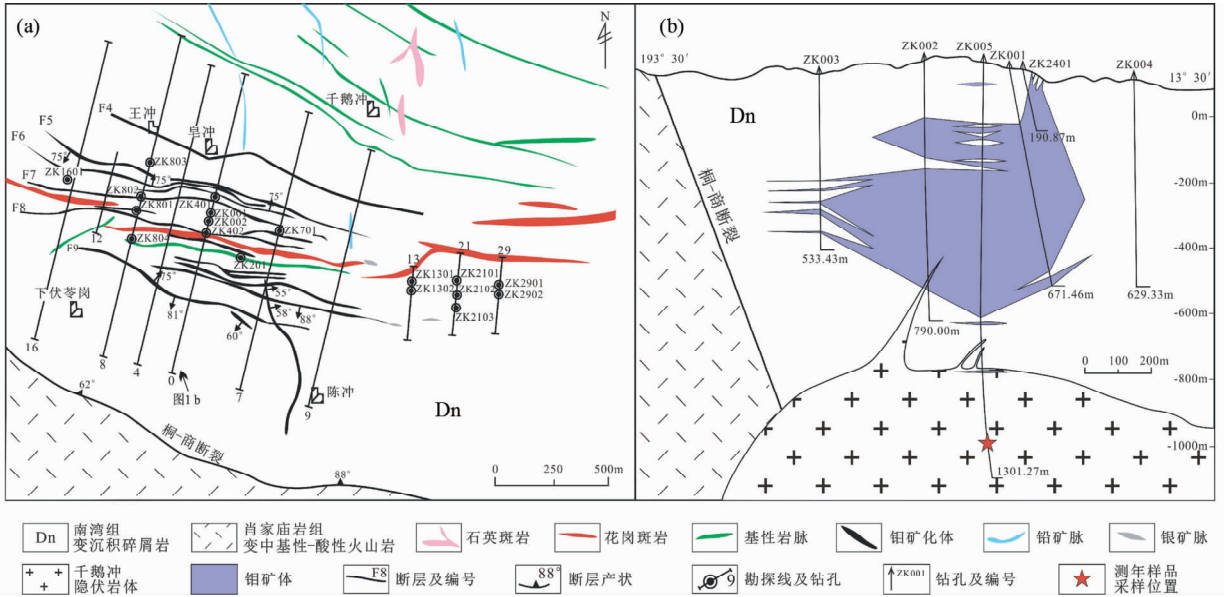


图2 千鹅冲钼矿地质简图及勘探线剖面图(据河南省地矿局第三地质调查队,2011^①)

Fig.2 Simplified geological map and cross-section of the Qian'echong Mo deposit

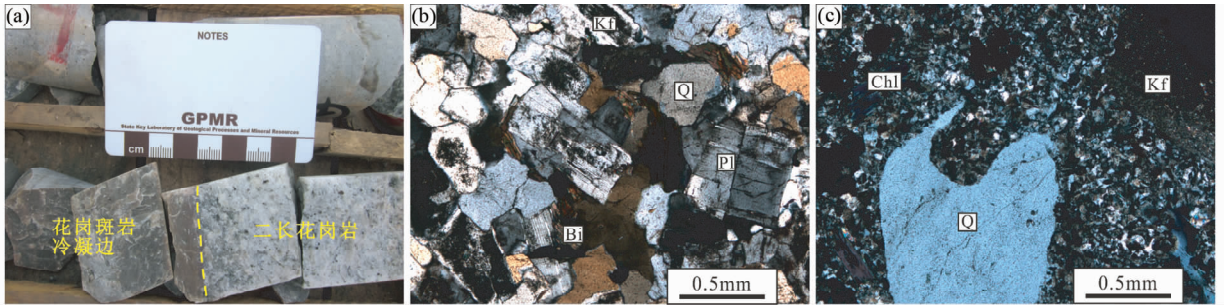


图3 千鹅冲岩体手标本及显微照片

(a)-二长花岗岩与花岗斑岩的侵入接触关系;(b)-二长花岗岩;(c)-花岗斑岩。Q-石英;Kf-钾长石;Pl-斜长石;Bi-黑云母;Chl-绿泥石

Fig.3 Hand specimens and photomicrographs showing petrology of Qian'echong stock

(a)-intrusive contact relationship of monzogranite and granite porphyry; (b)-monzogranite; (c)-granite porphyry. Q-quartz; Kf-K-feldspar; Pl-plagioclase; Bi-biotite; Chl-chloritic

云片岩、含绿帘二云石英片岩、黑云斜长石英片岩、黑云石英片岩等,矿体与围岩均呈渐变过渡关系,无明显界限。金属矿物主要为辉钼矿、黄铁矿、黄铜矿、方铅矿、闪锌矿、磁铁矿、赤铁矿等;脉石矿物主要为石英、钾长石、绿帘石、方解石、黑云母、绢云母、白云母、绿泥石、萤石。主要的矿石结构包括自形-半自形-他形结晶结构、交代结构、压碎结构、固溶体出溶结构等。矿石构造类型主要有脉状构造、浸染状构造、角砾状构造等。矿区内常见的围岩蚀变有硅化、钾长石化、黄铁矿化、绢云母化、绿帘石化、绿泥石化、碳酸盐化等,多叠加出现,强弱不等。以硅化、钾长石化、黄铁矿化、绢云母化发育较强。

4 样品描述及分析方法

本次研究所采集的二长花岗岩(QEC-7)和花岗斑岩(QEC-8)来自ZK005钻孔985m处,可见花岗斑岩在与二长花岗岩的接触部位有冷凝边(图3a),其形成晚于二长花岗岩。其中,二长花岗岩为灰白色,细粒结构,块状构造(图3b)。主要矿物为石英(20%~25%)、正长石(35%~40%)、斜长石(30%~35%);次要矿物为黑云母,含量2%~4%;副矿物主要有锆石、磷灰石、榍石、磁铁矿、铁钛矿等,

① 河南省地矿局第三地质调查队. 2011. 河南省光山县千鹅冲钼矿勘探报告

含量 1% ~ 3%。大部分岩石发生较强的硅化。花岗斑岩, 肉红色-暗红色, 斑状结构, 块状构造 (图 3c)。斑晶含量 15% ~ 20%, 主要为正长石 (40% ~ 50%)、石英 (35% ~ 40%)、斜长石 (15% ~ 20%) 及少量黑云母; 基质含量约为 80%, 矿物组成同斑晶, 粒度 0.1 ~ 0.4mm; 副矿物主要有磁铁矿、钛铁矿、锆石、磷灰石等, 含量为 1% ~ 5%。岩石普遍发生较强烈的钾硅酸盐化及硅化蚀变。

将岩石样品破碎, 经重力和磁选后在双目镜下挑选出锆石颗粒, 并与标准锆石一起置于环氧树脂做成样品靶, 进行锆石透、反射光、阴极发光照相, 以及 SHRIMP 定年、Lu-Hf 同位素分析和锆石微量元素测试。

锆石分选工作在廊坊市地源矿物测试分选技术服务有限公司完成。锆石阴极发光 (CL) 照相在中国地质科学院地质研究所北京离子探针中心完成。锆石 U-Pb 年龄数据是在中国地质科学院地质研究所北京离子探针中心的网络虚拟实验室, 通过 SHRIMP 远程共享控制系统 (SHRIMP Remote Operation System, SROS) 远程控制位于澳大利亚 Curtin 理工大学 (Curtin University of Technology) 的 SHRIMP II 仪器获得的, 详细测试方法见 Williams (1998)。SHRIMP 远程共享控制系统 (SROS) 由北京离子探针中心、中国计量科学研究院和吉林大学共同研发, 可以实现通过 Internet 公共网络, 远程控制 SHRIMP II 仪器、远程选取样品待测点和实时远程实验数据输出打印等功能。数据处理采用 SQUID 和 ISOPLOT 程序 (Ludwig, 2003)。

锆石 Lu-Hf 同位素测试是在中国地质科学院矿产资源研究所国土资源部成矿作用与资源评价重点实验室 Neptune 多接收等离子质谱和 Newwave UP213 紫外激光剥蚀系统 (LA-MC-ICP-MS) 上进行的, 实验过程中采用 He 作为剥蚀物质载气, 剥蚀直径为 55 μm , 测试时采用锆石国际标样 GJ1 作为参考物质, 分析点与 U-Pb 定年分析点为同一位置。相关

仪器运行条件及详细分析流程见侯可军等 (2007)。分析过程中锆石标准 GJ1 的 $^{176}\text{Hf}/^{177}\text{Hf}$ 测试加权平均值为 $0.282015 \pm 28 (2\sigma, n = 10)$, 与文献报道值 (侯可军等, 2007; Elhlou *et al.*, 2006) 在误差范围内完全一致。

锆石原位微量元素测试在国家地质实验测试中心 (NRCGA) 完成, 采用激光剥蚀等离子质谱 (LA-ICP-MS) 方法。使用仪器为 Thermo Element II 等离子质谱仪, 激光剥蚀系统为 New Wave UP-213。实验中采用 He 作为剥蚀物质的载气, 激光波长 213nm、束斑 40 μm 、脉冲频率 10Hz、能量 0.176mJ、密度 23 ~ 25J/cm², 测试过程中首先遮挡激光束进行空白背景采集 15s, 然后进行样品连续剥蚀采集 45s, 停止剥蚀后继续吹扫 15s 清洗进样系统, 单点测试分析时间 75s。等离子质谱测试参数为冷却气流速 (Ar) 15.55L/min; 辅助气流速 (Ar) 0.67L/min; 载气流速 (He) 0.58L/min; 样品气流速 0.819L/min, 射频发生器功率 1205W。数据测试标样使用 NIST-610。用于计算 Ce^{4+} 和 Ce^{3+} 在锆石-熔体中的分配系数所用到的全岩微量元素含量测试在国家地质实验测试中心完成, 检测仪器为等离子体质谱仪 ICP-MS (X-series), 测试精度优于 5%。

5 分析结果

5.1 SHRIMP 锆石 U-Pb 年龄

二长花岗岩 (QEC-7) 和花岗斑岩 (QEC-8) 中的锆石多呈柱状, 长度一般为 100 ~ 200 μm , 长宽比大多为 2 : 1 ~ 3 : 1, 无色透明, 具清晰震荡环带, 裂纹不发育, 显示岩浆成因特征 (Rubatto and Gebauer, 2000) (图 4)。本次研究中, 对样品 QEC-7 和 QEC-8 分别选择了 14 个和 16 个点进行测试, 锆石 U-Pb 定年结果列于表 1。两件样品中绝大部分锆石 Th/U 比值变化在 0.56 ~ 1.99 之间, 属典型岩浆锆石特征 (Belousova

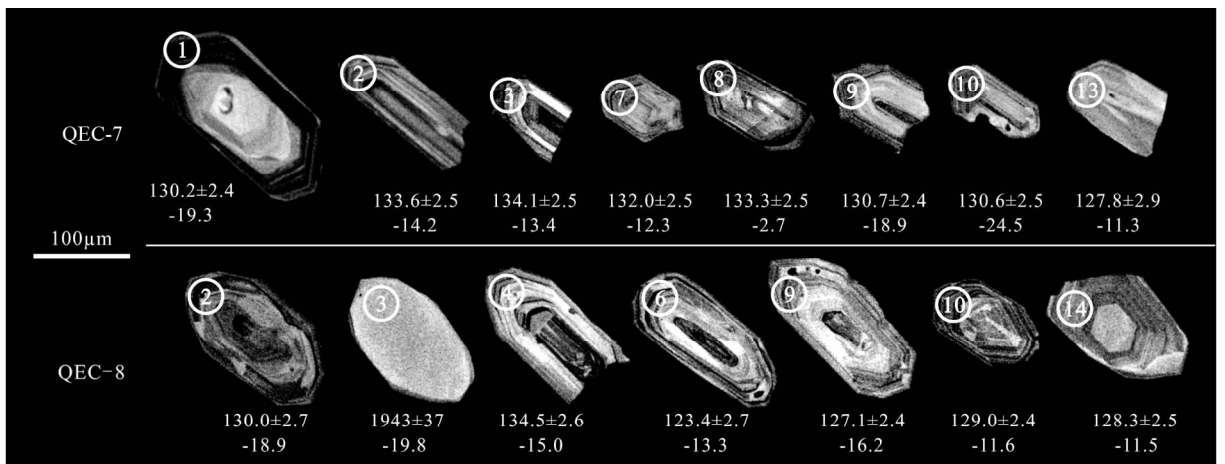


图 4 千鹅冲钼矿二长花岗岩和花岗斑岩代表性锆石阴极发光图像及测点位置、U-Pb 年龄和 $\epsilon_{\text{Hf}}(t)$ 值

Fig. 4 Cathodoluminescence (CL) images of representative zircon of monzogranite and granite porphyry from the Qian'echong Mo deposit with analytical numbers, U-Pb ages and $\epsilon_{\text{Hf}}(t)$

表1 千鹅冲钨矿床二长花岗岩(QEC-7)和花岗斑岩(QEC-8)的SHRIMP 锆石 U-Pb 同位素定年结果

Table 1 Results of SHRIMP zircon U-Pb dating of monzogranite (QEC-7) and granite porphyry (QEC-8) from the Qian'echong

Mo deposit

Spot No.	U ($\times 10^{-6}$)	Th ($\times 10^{-6}$)	Th/U	$^{206}\text{Pb}^*$ ($\times 10^{-6}$)	$^{206}\text{Pb}_c$ (%)	$^{207}\text{Pb}^*$ ^{235}U	$\pm\%$ (1σ)	$^{207}\text{Pb}^*$ $^{206}\text{Pb}^*$	$\pm\%$ (1σ)	$^{206}\text{Pb}^*$ ^{238}U	$\pm\%$ (1σ)	^{206}Pb ^{238}U Age(Ma)	$\pm\text{Ma}$ (1σ)
QEC-7-1.1	1682	944	0.58	29.5	0.15	0.1352	2.9	0.0481	2.2	0.0204	1.9	130.2	2.4
QEC-7-2.1	1248	1646	1.36	22.7	1.13	0.1420	7.6	0.0491	7.3	0.0210	1.9	133.6	2.5
QEC-7-3.1	1275	1078	0.87	23.0	—	0.1467	2.4	0.0506	1.5	0.0210	1.9	134.1	2.5
QEC-7-4.1	242	347	1.48	4.2	1.72	0.1102	8.8	0.0406	8.5	0.0197	2.1	125.8	2.6
QEC-7-5.1	365	494	1.40	6.1	1.23	0.1150	17	0.0431	17	0.0193	2.2	123.1	2.7
QEC-7-6.1	242	173	0.74	4.2	—	0.1637	4.3	0.0587	3.8	0.0202	2.1	129.1	2.7
QEC-7-7.1	1501	2047	1.41	26.8	0.26	0.1415	3.3	0.0496	2.7	0.0207	1.9	132.0	2.5
QEC-7-8.1	849	1410	1.72	15.3	0.36	0.1331	4.3	0.0462	3.9	0.0209	1.9	133.3	2.5
QEC-7-9.1	1548	1605	1.07	27.3	0.31	0.1438	3.0	0.0509	2.3	0.0205	1.9	130.7	2.4
QEC-7-10.1	1015	1851	1.89	17.7	—	0.1570	4.3	0.0556	3.9	0.0205	1.9	130.6	2.5
QEC-7-11.1	176	339	1.99	3.1	1.72	0.1100	19	0.0391	19	0.0204	2.3	130.1	3.0
QEC-7-12.1	500	401	0.83	8.6	0.50	0.1277	7.4	0.0464	7.1	0.0200	2.0	127.4	2.5
QEC-7-13.1	177	245	1.43	3.1	0.99	0.1210	15	0.0438	15	0.0200	2.3	127.8	2.9
QEC-7-14.1	1510	1118	0.77	26.7	0.38	0.1356	3.9	0.0479	3.5	0.0205	1.9	131.0	2.4
QEC-8-1.1	74	84	1.16	1.3	8.04	—	—	—	—	0.0193	4.0	123.2	4.9
QEC-8-2.1	408	332	0.84	7.1	—	0.172	10	0.0614	9.8	0.0204	2.1	130.0	2.7
QEC-8-3.1	58	33	0.58	17.4	—	6.4700	7.7	0.1334	7.4	0.3517	2.2	1943	37
QEC-8-4.1	467	0	0.00	8.5	0.82	0.1425	6.9	0.0490	6.6	0.0211	2.0	134.5	2.6
QEC-8-5.1	278	0	0.00	5.0	1.35	0.1110	13	0.0388	12	0.0207	2.1	132.1	2.7
QEC-8-6.1	798	0	0.00	13.2	—	0.1344	3.3	0.0504	2.5	0.0193	2.2	123.4	2.7
QEC-8-7.1	465	0	0.00	7.8	0.40	0.1729	3.3	0.0648	2.7	0.0194	2.0	123.5	2.4
QEC-8-8.1	643	749	1.20	11.1	0.48	0.1281	3.8	0.0467	3.3	0.0199	1.9	127.1	2.4
QEC-8-9.1	918	890	1.00	16.0	0.31	0.1349	5.6	0.0484	5.3	0.0202	1.9	129.0	2.4
QEC-8-10.1	1184	1541	1.34	20.7	—	0.1389	3.0	0.0494	2.4	0.0204	1.9	130.1	2.4
QEC-8-11.1	451	246	0.56	7.6	0.90	0.1240	11	0.0461	10	0.0195	2.0	124.7	2.5
QEC-8-12.1	1265	1085	0.89	21.9	0.26	0.1337	2.8	0.0482	2.1	0.0201	1.9	128.5	2.4
QEC-8-13.1	1668	1539	0.95	29.5	0.47	0.1279	4.3	0.0454	3.9	0.0205	1.9	130.5	2.4
QEC-8-14.1	450	293	0.67	7.8	—	0.1511	3.7	0.0545	3.1	0.0201	2.0	128.3	2.5
QEC-8-15.1	939	955	1.05	16.9	—	0.1415	2.6	0.0490	1.8	0.0209	1.9	133.6	2.5
QEC-8-16.1	2190	1514	0.71	40.7	3.45	0.1331	7.2	0.0463	6.9	0.0209	1.9	133.1	2.5

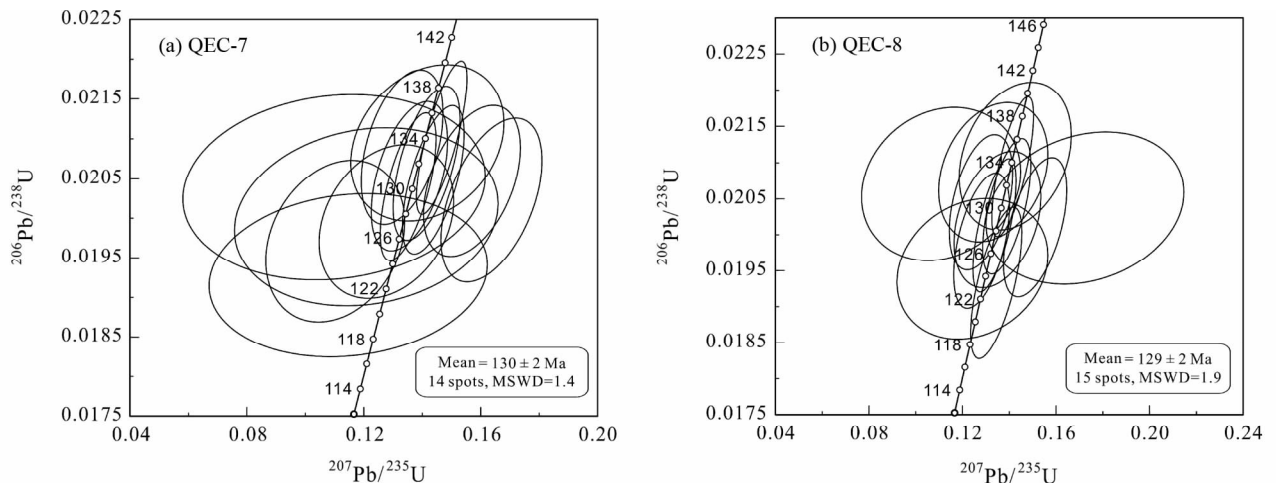
注: Pb^* 和 Pb_c 分别代表放射铅和普通铅, 锆石中的普通铅用实测 ^{204}Pb 校正; —表示未检出

图5 SHRIMP 锆石 U-Pb 年龄谐和图及加权平均年龄

Fig. 5 Zircon U-Pb isotope concordian diagrams and weighted average ages

表 2 千鹅冲钼矿床二长花岗岩(QEC-7)和花岗斑岩(QEC-8)锆石 Hf 同位素分析结果

Table 2 Zircon Hf isotopic composition of monzogranite (QEC-7) and granite porphyry (QEC-8) from the Qian'echong Mo deposit

Spot No.	$^{176}\text{Yb}/^{177}\text{Hf}$	$^{176}\text{Lu}/^{177}\text{Hf}$	$^{176}\text{Hf}/^{177}\text{Hf}$	$\pm 2\sigma$	$(^{176}\text{Hf}/^{177}\text{Hf})_i$	Age (Ma)	$\varepsilon_{\text{Hf}}(t)$	t_{DM1} (Ma)	t_{DM2} (Ma)
QEC-7-1.1	0.081111	0.001329	0.282149	0.000020	0.282146	130	-19.3	1568	2408
QEC-7-2.1	0.133935	0.002411	0.282295	0.000022	0.282289	134	-14.2	1403	2086
QEC-7-3.1	0.165089	0.003983	0.282320	0.000023	0.282310	134	-13.4	1428	2037
QEC-7-4.1	0.084447	0.001751	0.282234	0.000027	0.282229	126	-16.4	1465	2224
QEC-7-5.1	0.124646	0.001857	0.282278	0.000021	0.282273	123	-14.9	1406	2127
QEC-7-6.1	0.100361	0.001991	0.282274	0.000026	0.282270	129	-14.9	1417	2132
QEC-7-7.1	0.125645	0.001686	0.282346	0.000030	0.282342	132	-12.3	1303	1969
QEC-7-8.1	0.156112	0.002079	0.282618	0.000033	0.282612	133	-2.7	925	1362
QEC-7-9.1	0.087080	0.001311	0.282159	0.000028	0.282155	131	-18.9	1553	2385
QEC-7-10.1	0.074510	0.001296	0.282001	0.000024	0.281997	131	-24.5	1774	2736
QEC-7-11.1	0.087160	0.001234	0.282500	0.000028	0.282497	130	-6.9	1071	1624
QEC-7-12.1	0.135580	0.003162	0.282125	0.000029	0.282118	127	-20.4	1683	2470
QEC-7-13.1	0.096339	0.001378	0.282376	0.000031	0.282373	128	-11.3	1250	1902
QEC-7-14.1	0.119574	0.002989	0.282225	0.000020	0.282218	131	-16.7	1528	2245
QEC-8-1.1	0.118446	0.001641	0.282330	0.000025	0.282326	123	-13.1	1324	2010
QEC-8-2.1	0.081873	0.001279	0.282159	0.000022	0.282156	130	-18.9	1551	2385
QEC-8-3.1	0.013380	0.000196	0.280994	0.000019	0.280987	1,943	-19.8	3072	3787
QEC-8-4.1	0.066324	0.001110	0.282267	0.000019	0.282264	135	-15.0	1394	2142
QEC-8-5.1	0.039297	0.000600	0.282335	0.000025	0.282334	132	-12.6	1281	1988
QEC-8-6.1	0.107988	0.002129	0.282323	0.000022	0.282318	123	-13.3	1351	2027
QEC-8-7.1	0.079833	0.001154	0.282281	0.000021	0.282279	124	-14.7	1375	2116
QEC-8-8.1	0.069990	0.001097	0.282379	0.000018	0.282376	127	-11.2	1236	1895
QEC-8-9.1	0.071491	0.001184	0.282235	0.000021	0.282233	129	-16.2	1441	2215
QEC-8-10.1	0.108438	0.001996	0.282369	0.000019	0.282364	130	-11.6	1281	1921
QEC-8-11.1	0.102163	0.001578	0.282373	0.000024	0.282370	125	-11.5	1260	1912
QEC-8-12.1	0.075058	0.001339	0.282314	0.000019	0.282311	129	-13.5	1336	2041
QEC-8-13.1	0.081080	0.001531	0.282220	0.000018	0.282216	131	-16.8	1476	2250
QEC-8-14.1	0.084427	0.001238	0.282370	0.000024	0.282367	128	-11.5	1253	1915
QEC-8-15.1	0.135115	0.003077	0.282274	0.000025	0.282266	134	-14.9	1460	2136
QEC-8-16.1	0.105181	0.001756	0.282208	0.000026	0.282204	133	-17.2	1502	2276

注: $\varepsilon_{\text{Hf}}(t) = 10000 \times \{ [(^{176}\text{Hf}/^{177}\text{Hf})_s - (^{176}\text{Lu}/^{177}\text{Hf})_s \times (e^{\lambda t} - 1)] / [(^{176}\text{Hf}/^{177}\text{Hf})_{\text{CHUR},0} - (^{176}\text{Lu}/^{177}\text{Hf})_{\text{CHUR}} \times (e^{\lambda t} - 1)] - 1 \}$; $t_{\text{DM1}} = 1/\lambda \times \ln \{ 1 + [(^{176}\text{Hf}/^{177}\text{Hf})_s - (^{176}\text{Hf}/^{177}\text{Hf})_{\text{DM}}] / [(^{176}\text{Lu}/^{177}\text{Hf})_s - (^{176}\text{Lu}/^{177}\text{Hf})_{\text{DM}}] \}$; $t_{\text{DM2}} = 1/\lambda \times \ln \{ 1 + [(^{176}\text{Hf}/^{177}\text{Hf})_s - (^{176}\text{Hf}/^{177}\text{Hf})_{\text{DM},t}] / [(^{176}\text{Lu}/^{177}\text{Hf})_e - (^{176}\text{Lu}/^{177}\text{Hf})_{\text{DM}}] \} + t$; $(^{176}\text{Lu}/^{177}\text{Hf})_s$ 和 $(^{176}\text{Hf}/^{177}\text{Hf})_s$ 为样品测定值; $(^{176}\text{Hf}/^{177}\text{Hf})_{\text{CHUR},0} = 0.282772$, $(^{176}\text{Lu}/^{177}\text{Hf})_{\text{CHUR}} = 0.0332$, $(^{176}\text{Hf}/^{177}\text{Hf})_{\text{DM}} = 0.28325$, $(^{176}\text{Lu}/^{177}\text{Hf})_{\text{DM}} = 0.0384$ (Blichert-Toft and Albarède, 1997; Griffin *et al.*, 2000); $\lambda = 1.867 \times 10^{-11}/\text{a}$ (Soderlund *et al.*, 2004); $(^{176}\text{Lu}/^{177}\text{Hf})_e = 0.015$; t 为锆石结晶时间

et al., 2002)。QEC-7 的 14 个测试点和 QEC-8 的 15 个测试点分别得到 $^{206}\text{Pb}/^{238}\text{U}$ 年龄为 $130 \pm 2\text{Ma}$ (MSWD = 1.4) 和 $129 \pm 2\text{Ma}$ (MSWD = 1.9) (图 5), 分别代表二长花岗岩和花岗斑岩的结晶年龄。另外, 样品 QEC-8 中的一个测点 3.1 得到了 $1943 \pm 37\text{Ma}$ 的年龄, 没有参与加权平均年龄的计算。以上测年结果显示千鹅冲隐伏岩体中的二长花岗岩和花岗斑岩形成于同一岩浆事件。

5.2 锆石 Hf 同位素

在 SHRIMP 锆石 U-Pb 定年的基础上, 对样品 QEC-7 和 QEC-8 进行了锆石微区 Hf 同位素测定, 分析结果见表 2 和

图 6。大部分锆石的 $^{176}\text{Lu}/^{177}\text{Hf}$ 比值小于 0.002, 说明锆石在形成后具有很少的放射成因 Hf 的积累, 所测定的 $^{176}\text{Hf}/^{177}\text{Hf}$ 比值基本代表了其形成时体系的 Hf 同位素组成。样品 QEC-7 共分析 14 个点, $^{176}\text{Hf}/^{177}\text{Hf}$ 比值变化于 0.282001 ~ 0.282618, $\varepsilon_{\text{Hf}}(t)$ 值变化于 -24.5 ~ -2.7 (绝大部分集中在 -24.5 ~ -11.3 之间), 两阶段模式年龄 (t_{DM2}) 变化于 1362 ~ 2736Ma。样品 QEC-8 共分析 16 个点, $^{176}\text{Hf}/^{177}\text{Hf}$ 比值变化于 0.280994 ~ 0.282379, $\varepsilon_{\text{Hf}}(t)$ 值较均一, 变化于 -19.8 ~ -11.2, 除一颗继承锆石的两阶段模式年龄 (t_{DM2}) 为 3787Ma 外, 其他变化于 1895 ~ 2385Ma 之间 (图 6)。

表3 千鹅冲钼矿二长花岗岩和花岗斑岩锆石微量元素 LA-ICP-MS 测试结果 ($\times 10^{-6}$)Table 3 Zircon trace element data of monzogranite and granite porphyry in the Qian'echong Mo deposit ($\times 10^{-6}$)

测点号	La	Ce	Pr	Nd	Sm	Eu	Gd	Tb	Dy	Ho	Er	Tm	Yb	Lu	Th	U	Hf
QEC-7(二长花岗岩)																	
1	0.02	26.0	0.05	0.75	2.56	1.09	10.8	3.45	51.9	20.8	106	20.2	286	58.5	83.4	342	17431
2	0.41	122	0.89	8.51	12.8	4.42	57.8	15.6	194	96.1	442	71.0	760	169	961	1888	21684
3	2.83	82.3	1.70	9.36	11.3	3.03	40.8	13.0	188	76.2	358	62.5	712	151	673	1738	19416
4	0.20	94.4	0.36	3.29	6.48	1.94	34.8	10.3	147	68.1	363	67.7	738	168	1066	1623	19244
5	2.73	133	3.65	24.1	23.4	6.67	74.9	21.7	241	90.7	422	85.7	853	190	1269	2086	18515
6	0.09	93.8	0.29	2.37	3.38	1.47	23.3	8.07	101	48.2	287	50.2	519	118	778	858	16822
7	0.05	32.3	0.09	0.59	1.63	1.06	8.61	2.85	35.2	16.7	77.6	13.5	137	31.6	117	194	19377
8	0.96	132	0.73	6.59	13.2	3.70	45.7	12.9	147	61.6	249	38.9	378	70.6	1143	955	14728
9	3.84	167	2.18	11.4	11.7	4.53	51.9	17.2	215	87.9	437	82.7	864	187	1657	2415	17589
10	1.00	118	0.83	9.16	14.0	5.65	57.6	18.4	196	72.5	308	55.7	580	103	727	741	11072
11	1.13	47.9	0.84	6.52	8.29	2.21	33.8	9.85	129	54.0	240	41.6	412	89.5	385	1336	17901
12	2.64	156	2.08	19.2	27.2	10.6	122	31.6	344	127	556	90.8	796	143	998	891	12897
13	0.29	151	1.14	13.3	25.3	5.40	94.9	26.2	293	114	495	78.9	752	152	1350	1295	14638
14	2.03	461	2.23	18.2	29.2	10.4	123	30.2	313	133	575	81.7	640	117	2332	957	14226
15	4.47	126	1.55	10.3	17.6	6.78	51.2	14.2	183	77.7	287	46.5	534	121	953	1321	19386
16	0.23	81.0	1.07	12.4	25.5	10.0	86.9	21.0	247	95.4	382	57.2	586	120	344	396	16506
17	6.03	195	2.31	9.04	11.4	5.23	54.9	14.4	153	68.5	285	38.2	337	59.2	691	379	16054
全岩	60.4	94.4	9.03	29.0	3.87	0.69	2.63	0.30	1.51	0.22	0.66	0.10	0.49	0.08	22.9	4.35	4.69
QEC-8(花岗斑岩)																	
1	0.18	74.2	0.95	14.1	27.4	7.64	72.0	21.9	257	90.9	319	52.1	533	98.7	387	246	12223
2	0.14	69.8	0.22	2.07	4.95	1.88	21.1	5.80	78.5	37.1	188	29.9	340	78.3	321	380	17923
3	0.04	21.0	0.13	1.34	2.90	0.63	11.5	2.94	34.3	14.9	65.9	9.56	86.7	17.2	35.6	80.7	18603
4	102	365	31.3	107	29.8	7.30	51.8	13.7	146	52.2	256	46.9	498	80.9	780	932	13114
5	0.11	20.7	0.63	8.09	11.3	3.67	42.3	10.2	107	44.6	177	29.9	255	45.6	114	110	12688
6	6.56	133	1.47	8.88	12.5	3.70	52.9	15.5	205	89.7	396	60.6	576	125	595	627	15314
7	3.77	91.2	4.28	17.7	9.54	2.69	30.2	8.05	98.3	42.4	225	35.8	359	77.8	451	652	15181
8	45.3	193	23.9	76.7	24.8	3.11	54.1	12.5	146	61.1	272	41.6	393	78.7	397	826	17922
9	125	373	35.7	126	32.4	6.14	60.0	14.1	163	72.4	319	49.2	426	90.6	411	446	15005
10	41.6	142	9.75	41.8	22.2	4.32	55.2	16.1	206	73.7	291	49.9	502	92.1	305	320	10863
11	4.51	84.2	1.68	10.6	11.3	3.07	45.8	13.4	163	67.3	309	56.2	519	92.3	427	452	12926
12	29.5	123	7.21	29.6	15.0	2.07	46.7	15.3	186	66.1	284	53.2	565	92.0	962	1260	11256
13	5.66	110	4.28	18.1	18.0	5.92	51.3	13.5	148	69.8	324	52.8	549	141	736	938	22108
14	0.14	37.3	0.32	4.09	7.03	0.58	30.2	9.28	124	48.6	220	36.6	380	75.5	302	592	14122
15	0.55	45.1	0.33	2.86	3.88	1.60	19.6	6.00	83.8	48.7	255	45.4	528	145	680	1474	19242
16	6.32	78.5	2.10	11.7	8.41	2.69	28.4	8.40	109	44.0	211	38.4	428	98.6	642	1039	14575
17	1.95	74.3	1.34	12.1	16.4	4.21	72.4	20.6	220	81.1	361	61.4	576	100	476	489	13029
18	0.59	58.3	0.40	3.26	4.99	1.86	26.6	8.30	104	44.4	223	38.7	355	66.0	333	370	14067
19	3.67	68.9	2.02	10.9	10.3	3.17	40.5	11.3	137	58.6	277	45.2	444	93.2	729	809	14297
20	5.12	39.5	2.82	16.5	17.8	0.69	79.3	19.2	192	72.8	339	57.4	471	77.6	338	562	15152
全岩	41.6	67.7	6.53	21.0	3.08	0.56	2.30	0.34	1.76	0.29	0.85	0.14	0.92	0.17	26.9	7.46	4.77

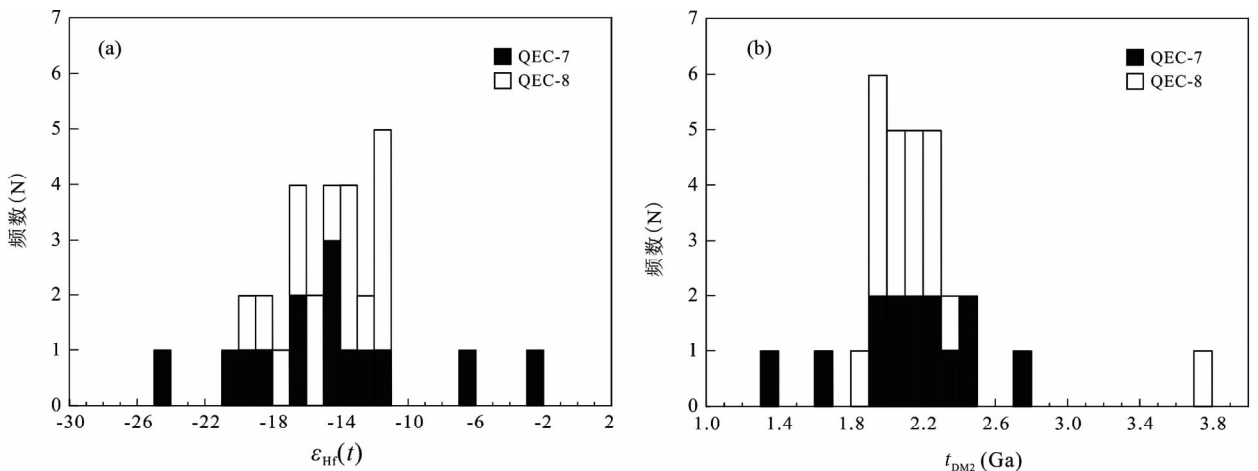
图6 二长花岗岩和花岗斑岩锆石 $\epsilon_{\text{Hf}}(t)$ 统计直方图(a)和二阶段模式年龄(t_{DM2})统计直方图(b)Fig. 6 Histogram of $\epsilon_{\text{Hf}}(t)$ (a) and two stage mode ages (t_{DM2}) (b) of zircons from monzogranite and granite porphyry

表4 千鹅冲钼矿二长花岗岩和花岗斑岩锆石 Ce^{3+} 和 Ce^{4+} 的分配系数及比值

Table 4 Partition coefficients and ratios of Ce^{3+} and Ce^{4+} of zircons from monzogranite and granite porphyry in the Qian'echong Mo deposit

测点号	$D_{Ce^{3+}}$	$D_{Ce^{4+}}$	Ce^{4+}/Ce^{3+}	Ce/Ce^*	Eu/Eu^*
QEC-7(二长花岗岩)					
1	0.00070	341.5	393.7	234.6	0.63
2	0.00600	803.5	215.3	49.7	0.50
3	0.00529	720.2	164.0	9.2	0.43
4	0.00157	847.4	636.1	85.5	0.39
5	0.01730	896.3	80.6	10.3	0.49
6	0.00062	758.9	1606	145.2	0.51
7	0.00053	384.2	639.3	115.1	0.87
8	0.01533	870.3	90.6	38.7	0.46
9	0.00462	999.4	382.5	14.1	0.56
10	0.01202	739.6	103.1	31.8	0.61
11	0.00481	584.7	104.5	12.1	0.40
12	0.03290	823.7	49.4	16.4	0.57
13	0.02630	938.3	60.0	63.9	0.34
14	0.04600	1103.9	105.7	53.2	0.53
15	0.01552	808.5	85.3	11.8	0.69
16	0.03346	551.6	24.7	40.2	0.65
17	0.01412	708.2	145.8	12.8	0.64
QEC-8(花岗斑岩)					
1	0.15925	541.9	5.9	43.7	0.53
2	0.00648	508.1	158.4	98.2	0.56
3	0.01032	226.7	29.1	75.7	0.33
4	0.21304	652.2	24.5	1.6	0.57
5	0.05883	344.0	4.2	19.7	0.51
6	0.02666	617.8	72.9	10.5	0.44
7	0.02364	576.7	56.1	5.6	0.49
8	0.15398	521.4	17.6	1.4	0.26
9	0.22445	543.4	23.8	1.4	0.43
10	0.11094	483.7	17.9	1.7	0.38
11	0.02921	548.7	41.7	7.5	0.41
12	0.05154	745.4	34.4	2.1	0.24
13	0.04518	673.2	34.9	5.5	0.59
14	0.01412	490.2	38.0	42.9	0.12
15	0.00213	675.9	311.3	25.9	0.56
16	0.01469	658.5	78.0	5.3	0.53
17	0.05755	584.1	18.1	11.3	0.37
18	0.00824	497.5	103.6	29.5	0.49
19	0.02369	662.0	42.0	6.2	0.47
20	0.08648	499.7	5.7	2.5	0.06

注: 锆石和熔体之间 Ce^{4+} 和 Ce^{3+} 的分配系数 $D_{Ce^{3+}}$ 、 $D_{Ce^{4+}}$ 及 Ce^{4+}/Ce^{3+} 比值计算方法据 Ballard *et al.* (2002); $Eu/Eu^* = Eu_N / (Sm_N \times Gd_N)^{1/2}$; $Ce/Ce^* = Ce_N / (La_N \times Pr_N)^{1/2}$

5.3 锆石微量元素特征

锆石中稀土元素及 Th、U、Hf 元素含量见表 3。测试结果显示, 二长花岗岩中锆石的稀土总量为 $358.9 \times 10^{-6} \sim 2536 \times 10^{-6}$, 平均为 1604×10^{-6} ; 花岗斑岩中锆石的稀土总

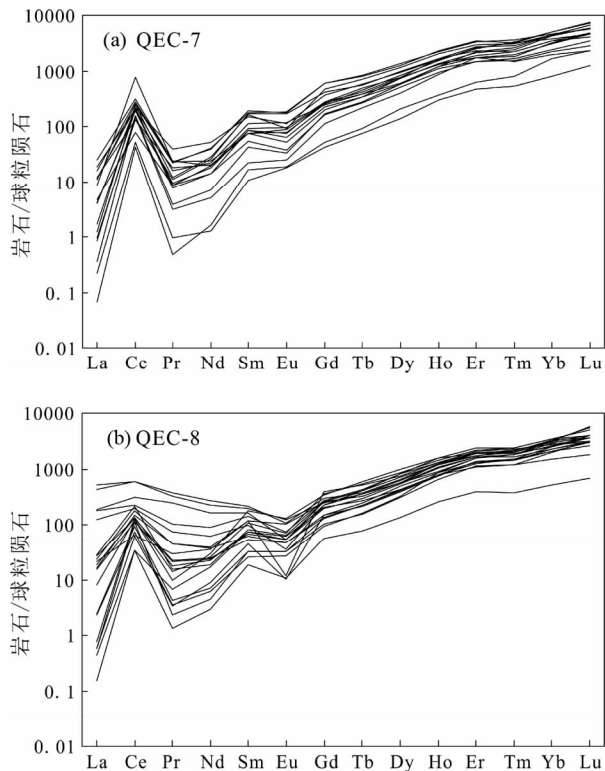


图7 锆石稀土元素球粒陨石标准化配分曲线(球粒陨石标准化值据 Sun and McDonough, 1989)

Fig. 7 Chondrite-normalized REE patterns of zircons (chondritite values after Sun and McDonough, 1989)

量为 $268.8 \times 10^{-6} \sim 1893 \times 10^{-6}$, 平均为 1279×10^{-6} 。锆石稀土元素球粒陨石标准化配分曲线(图 7)显示, 二长花岗岩和花岗斑岩具有较一致的稀土元素特征, 亏损 LREE 且富集 HREE。

锆石 Ce^{4+} 和 Ce^{3+} 在锆石-熔体间的分配系数 $D_{Ce^{4+}}$ 、 $D_{Ce^{3+}}$ 及 Ce^{4+}/Ce^{3+} 比值见表 4。计算结果显示, 二长花岗岩和花岗斑岩都具有变化较大的 Ce^{4+}/Ce^{3+} 比值, 但二长花岗岩总体上具有相对花岗斑岩更大的 Ce^{4+}/Ce^{3+} 比值。二长花岗岩和花岗斑岩中的锆石均显示正 Ce 异常和 Eu 负异常(图 7), 但样品 QEC-8 中部分锆石具有更强负 Eu 异常(图 7b), 锆石 Ce/Ce^* 分别变化于 9.2 ~ 234.6 和 1.4 ~ 98.2 之间, Eu/Eu^* 变化范围分别为 0.34 ~ 0.87 (平均 0.55) 和 0.06 ~ 0.59 (平均 0.42)。

6 讨论

6.1 成岩成矿时代

本次研究得到千鹅冲钼矿中隐伏的二长花岗岩和花岗斑岩 SHRIMP 锆石 U-Pb 年龄分别为 $130 \pm 2Ma$ 和 $129 \pm 2Ma$, 二者在误差范围内一致。这一结果与李法岭(2011)和杨梅珍等(2010)报道的千鹅冲钼矿床的辉钼矿 Re-Os 同位

素年龄($128 \pm 7\text{Ma}$)及成矿后花岗斑岩脉的年龄($129 \pm 3\text{Ma}$)也具有比较好的一致性,说明千鹅冲斑岩型钼矿床的成矿作用发生在早白垩世。

鉴于前人(李法岭,2011;杨梅珍等,2010)报道的千鹅冲钼矿辉钼矿 Re-Os 等时线年龄误差较大($\pm 7\text{Ma}$),最近,作者运用辉钼矿 Re-Os 同位素定年重新厘定了千鹅冲钼矿的成矿时代,6 件辉钼矿样品得到了一条理想的等时线,其 Re-Os 等时线年龄为 $129 \pm 2\text{Ma}$ (MSWD = 0.63) (数据待发表)。这一结果与本文获得的千鹅冲矿区二长花岗岩和花岗斑岩的 SHRIMP 锆石 U-Pb 年龄非常一致,说明千鹅冲钼矿成矿成矿时限较短,约为 $128 \sim 130\text{Ma}$ 。

近年来,东秦岭-大别钼矿带钼矿床年代学研究表明,虽然有少量钼矿床形成于中生代以前(如塞凹和龙门店,李厚民等,2009;魏庆国等,2009),但总体上以中生代成矿作用大爆发为显著特征(李永峰等,2005;毛景文等,2005;叶会寿等,2006)。Mao *et al.* (2008,2011a) 比较全面地统计了东秦岭-大别钼矿带钼矿床成矿时代,将中生代钼矿床作用划分为三个期次:晚三叠($221 \sim 233\text{Ma}$)、晚侏罗-早白垩($138 \sim 148\text{Ma}$)、早-中白垩($112 \sim 131\text{Ma}$)。与东秦岭多期次钼成矿作用不同,除个别侏罗纪年龄外,绝大多数大别山地区钼矿床的成矿作用发生于早白垩世(黄凡等,2011;李毅等,2013,及其中引文),此时代跨度与大别山碰撞后岩浆作用时限基本一致(He *et al.*, 2011;Wang *et al.*, 2007)。

6.2 岩浆源区及相对氧逸度

6.2.1 岩浆源区

锆石 Lu-Hf 同位素体系具有较高的封闭温度(Scherer *et al.*, 2000),能有效地揭示岩浆演化过程和源区性质(Griffin *et al.*, 2000;Beloisova *et al.*, 2006)。由于 Hf 属于不相容元素,当寄主岩浆不断发生部分熔融和结晶分异作用时,亏损地幔源区具有更高的 $^{176}\text{Hf}/^{177}\text{Hf}$ 比值,使得熔融物和寄主岩浆发生 $^{176}\text{Hf}/^{177}\text{Hf}$ 比值的解耦,即大陆地壳相对于亏损地幔具有更低的 $^{176}\text{Hf}/^{177}\text{Hf}$ 比值和 $\varepsilon_{\text{Hf}}(t)$ 值(Patchett *et al.*, 1981)。

表 2 和图 8 显示,千鹅冲钼矿中二长花岗岩和花岗斑岩中的锆石具有低的 $\varepsilon_{\text{Hf}}(t)$ 值和古老的 Hf 模式年龄,并且所有 Hf 同位素数据点均落于球粒陨石 Hf 同位素演化线之下(图 8),表明千鹅冲岩体主要来源于古老的地壳物质。大别造山带的深部地壳和岩石圈地幔是否存在华北物质存在争议(Huang *et al.*, 2007;Li and Yang, 2003;Wang *et al.*, 2005),但基于对大别造山带超高压变质岩及早白垩世高 Sr/Y 花岗岩的地球化学性质的详细研究,多数学者认为大别造山带的地壳物质基本来自华南板块(He *et al.*, 2013;Zheng *et al.*, 2003;Zheng and Zhang, 2007;Zhao *et al.*, 2007;Zhao and Zheng, 2009)。所以千鹅冲花岗岩应来源于华南板块边缘的古老地壳。

千鹅冲花岗岩的锆石 Hf 同位素特征与大别造山带碰撞

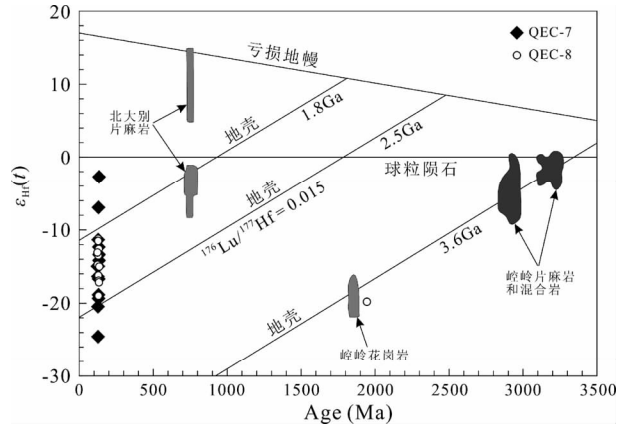


图 8 锆石 $\varepsilon_{\text{Hf}}(t)$ -Age 图解

资料来源:北大别片麻岩引自 Zhao *et al.* (2008);太古代崆岭片麻岩和混合岩以及古元古代崆岭花岗岩引自 Zhang *et al.* (2006),Zheng *et al.* (2006),Xiong *et al.* (2008);亏损地幔演化线据 Nowell *et al.* (1998)

Fig. 8 $\varepsilon_{\text{Hf}}(t)$ vs. Age plots for zircons

Data sources: The granitic gneiss from North Dabie from Zhao *et al.* (2008); Archean gneiss and migmatite and Paleoproterozoic granite from the Kongling Complex from Zhang *et al.* (2006a); Zheng *et al.* (2006b); Xiong *et al.* (2008). The evolutionary line of depleted mantle after Nowell *et al.* (1998)

后花岗岩的锆石 Hf 同位素特征具有相似性(Zhao *et al.*, 2011),暗示它们具有一致的来源。对大别造山带内碰撞后花岗岩类的研究表明,它们与造山带地表出露的原岩为新元古代的双峰式火成岩的高压-超高压变质岩(Liu and Xue, 2007;Zheng *et al.*, 2003)有相似的地球化学特征(Bryant *et al.*, 2004;He *et al.*, 2011, 2013;Wang *et al.*, 2007;Zhang *et al.*, 2002;Zhao *et al.*, 2011),说明这些花岗岩来自大别造山带高压-超高压变质岩的部分熔融(He *et al.*, 2013;Wang *et al.*, 2007;Zhao *et al.*, 2011)。虽然对于大别造山带后碰撞花岗岩具体来自镁铁质榴辉岩还是中酸性大别片麻岩存在较大分歧(He *et al.*, 2011, 2013;Wang *et al.*, 2007;Zhao *et al.*, 2011;Xu *et al.*, 2013),但是古元古-太古代的继承锆石、古元古-太古代的 Nd 和 Hf 的模式年龄都指示这些花岗岩的原岩混入了不同比例的更古老的地壳物质(如太古代崆岭杂岩)(He *et al.*, 2013;Zhao *et al.*, 2011)。千鹅冲花岗斑岩中发现了年龄为 1943Ma 的古元古代继承锆石,其与崆岭杂岩内的古元古代花岗岩具有相似的 Hf 同位素特征(图 8),也说明了其原岩混入了类似崆岭杂岩的古老地壳物质。虽然两个样品中大部分锆石的 $\varepsilon_{\text{Hf}}(t)$ 值为较低的值,但是变化范围较大的 $\varepsilon_{\text{Hf}}(t)$ 值和二阶段模式年龄暗示其源区可能混入了不同比例的年轻地幔组分,尤其是二长花岗岩(图 6)。大别山地区白垩纪超基性岩浆作用开始于 $\sim 130\text{Ma}$ (Jahn *et al.*, 1999;Wang *et al.*, 2005),说明此时地幔上涌不仅为花岗岩原岩部分熔融提供了热源,也注入了少量幔源

组分。

6.2.2 相对氧逸度

实验表明, Mo 在流体中的溶解度与流体的氧逸度关系密切 (Bali *et al.*, 2012)。岩浆中的 Ce 常呈 3 价和 4 价, 在氧化条件下, 锆石中的 Zr^{4+} 容易被 Ce^{4+} 离子取代。另外, Ce^{3+} 和 Ce^{4+} 的分异能力很强, 对岩浆的氧化还原状态具有较高的敏感度, 因此可以通过 Ce^{4+}/Ce^{3+} 比值来判断岩浆氧逸度的相对高低 (Ballard *et al.*, 2002; Bolhar *et al.*, 2008; Burnham and Berry, 2012; Trail *et al.*, 2012)。Eu 在岩浆中呈 Eu^{2+} 和 Eu^{3+} 两种价态, 当 Ce^{4+} 稳定存在时, Eu 应呈三价。实验表明, Eu 的异常一般与 Ce 的异常呈正相关关系, 并且也可用来指示熔体的氧逸度 (Burnham and Berry, 2012; Trail *et al.*, 2012)。

千鹅冲钼矿花岗斑岩中的锆石比二长花岗岩中的锆石具有更低的 Eu/Eu^* 比值, 即更强的 Eu 异常, 可能是由于斜长石的分离结晶作用 (Hoskin and Schaltegger, 2003)。随着岩浆的演化, 在锆石达到饱和之前, Eu^{2+} 优先进入斜长石, 从而造成了演化程度更高的花岗斑岩中的锆石具有更强的 Eu 异常。二长花岗岩和花岗斑岩中的锆石的 Ce^{4+}/Ce^{3+} 比值平均值分别为 287.4 和 55.9。二长花岗岩中的锆石中具有较高的 Ce^{4+}/Ce^{3+} 比值, 与西藏玉龙和冈底斯地区以及智利东部的斑岩铜矿具有相似的特征 (Ballard *et al.*, 2002; Liang *et al.*, 2006; 辛洪波和曲晓明, 2008), 相比之下, 花岗斑岩中锆石的 Ce^{4+}/Ce^{3+} 比值明显低于这些斑岩铜矿。钻孔中揭露的花岗斑岩远多于二长花岗岩且形成晚于二长花岗岩, 推测成矿流体更可能来自花岗斑岩。已有研究表明, 岩浆的氧逸度不是控制钼成矿的决定因素, 岩浆中铁和钛的含量、岩浆流体含量以及岩浆上升过程中的对流机制都是影响钼富集的重要因素 (Keppler and Wyllie, 1991; Shinogara *et al.*, 1995; Tacker and Candela, 1987)。

6.3 动力学背景

大别造山带形成于三叠纪华南与华北板块之间的碰撞对接 (Li *et al.*, 1993; Hacker *et al.*, 1998), 关于造山带内含柯石英和金刚石的超高压变质岩的研究显示大量的华南陆壳物质曾深俯冲到超过 100km 的深度 (Wang *et al.*, 1989)。然而, 地震资料表明该造山带现今地壳的平均厚度约为 35km, 且缺少基性下地壳, 暗示曾经发生了加厚山根的拆沉作用 (Gao *et al.*, 1998a, b)。

大别造山带发育的大量白垩纪花岗岩在约 130Ma 发生明显的地球化学特征变化, 即 >130Ma 形成的花岗岩具有高 Sr/Y 和 $(La/Yb)_N$ 比值以及低 Y 含量的特征, 而形成于 130Ma 之后的花岗岩则不具备这一特征 (He *et al.*, 2011; Wang *et al.*, 2007)。研究表明, 早期花岗岩 (130 ~ 143Ma) 来自石榴石为主要残留相的加厚下地壳的部分熔融 (He *et al.*, 2011)。花岗岩地球化学特征在 130Ma 左右发生的转变指示大别造山带在约 130Ma 发生了下地壳的拆沉作用, 所以

之后形成的花岗岩来自减薄地壳的部分熔融 (He *et al.*, 2011; Wang *et al.*, 2007; Xu *et al.*, 2007)。另外, 北大别广泛分布的形成于 123 ~ 130Ma 的镁铁-超镁铁质岩的地球化学特征显示, 它们具有明显的陆壳物质特征属性, 可能由拆沉的下地壳熔体交代上地幔或岩石圈地幔形成 (Huang *et al.*, 2007)。所以, 大别造山带在早白垩世发生了下地壳的拆沉作用 (Gao *et al.*, 1998a, b)。

碰撞造山带的演化一般都要经历从挤压缩短向伸展减薄的构造体制的转换过程 (Leech, 2001; Vanderhaeghe and Teyssier, 2001)。大别造山带早白垩世下地壳拆沉作用可能导致造山带的去山根作用、软流圈上涌及大规模地壳伸展 (Ratschbacher *et al.*, 2000, 2003; Bryant *et al.*, 2004; Hacker *et al.*, 2004; Liu *et al.*, 2004)。Wu *et al.* (2007) 通过对北大别混合岩的研究认为, 大别山地区构造体制由挤压向伸展转换的时间约为 145Ma。另外, 大别造山带于早白垩世侵位的 A 型花岗岩也进一步证明了当时的伸展环境 (王强等, 2000; 谢智等, 2004)。

综上所述, 千鹅冲钼矿的成岩成矿作用发生在大别山地区早白垩世的伸展构造背景下。事实上, 整个中国东部在早白垩世总体处在伸展的构造体制下 (Mao *et al.*, 2011b; Wang *et al.*, 2012)。在这一时期, 不仅形成了东秦岭-大别钼矿带这一世界级钼多金属成矿省 (Mao *et al.*, 2008, 2011a), 而且在中国东北地区 (Yang *et al.*, 2003; 孙景贵等, 2012)、华北克拉通内部 (翟明国, 2010; 毛景文等, 2005)、长江中下游地区 (Duan *et al.*, 2012; Mao *et al.*, 2011c; Xie *et al.*, 2008, 2011, 2012; 袁顺达等, 2010) 以及华南地区 (Mao *et al.*, 2013) 均发育了大规模的构造-岩浆-成矿事件 (Mao *et al.*, 2011b; Wang *et al.*, 2012; Wu *et al.*, 2005), 它们均与中国东部乃至亚洲东北部晚中生代大规模地壳伸展的构造背景密切相关 (Mao *et al.*, 2003; Wang *et al.*, 2012)。

7 结论

(1) 千鹅冲钼矿区隐伏岩体中的二长花岗岩和花岗斑岩的 SHRIMP 锆石 U-Pb 年龄分别为 $130 \pm 2Ma$ 和 $129 \pm 2Ma$, 与辉钼矿 Re-Os 年龄一致, 为早白垩世, 成岩成矿作用发生在一个很短的时限内 (128 ~ 130Ma)。

(2) 锆石 Hf 同位素特征显示千鹅冲岩体的物质来源主要为华南陆块北缘的古老地壳及少量年轻地幔组分, 原岩中含有古元古代-太古代的基底岩石, 二长花岗岩相比花岗斑岩具有更高的氧逸度。

(3) 千鹅冲钼矿床形成于早白垩世的伸展构造体制下。大别造山带于早白垩世发生的下地壳拆沉作用导致的软流圈上涌及壳幔相互作用不仅形成了大规模的岩浆作用, 也为斑岩型钼矿床提供了物质来源。

致谢 中国地质科学院地质研究所刘建辉、矿产资源研究

所郭春丽和国家地质实验测试中心孙东阳分别在 SHRIMP 锆石测年、锆石 Hf 同位素测试及锆石微量元素测试过程中提供了大量帮助,在此一并表示感谢。

References

- Bali E, Keppler H and Audetat A. 2012. The mobility of W and Mo in subduction zone fluids and the Mo-W-Th-U systematics of island arc magmas. *Earth and Planetary Science Letters*, 351–352: 195–207
- Ballard J, Palin M and Campbell I. 2002. Relative oxidation states of magmas inferred from Ce(IV)/Ce(III) in zircon: Application to porphyry copper deposits of northern Chile. *Contributions to Mineralogy and Petrology*, 144(3): 347–364
- Beloisova BA, Griffin WL and O'Reilly SY. 2006. Zircon crystal morphology, trace element signatures and Hf Isotope composition as a tool for petrogenetic modeling: Examples from Eastern Australian granitoids. *Journal of Petrology*, 47(2): 329–353
- Belousova EA, Griffin WL, O'Reilly SY and Fisher NI. 2002. Igneous zircon: Trace element composition as an indicator of source rock type. *Contributions to Mineralogy and Petrology*, 143(5): 602–622
- Blichert-Toft J and Albarède F. 1997. The Lu-Hf isotope geochemistry of chondrites and the evolution of the mantle-crust system. *Earth and Planetary Science Letters*, 148: 243–258
- Bolhar R, Weaver SD, Palin JM, Cole JW and Paterson LA. 2008. Systematics of zircon crystallisation in the Cretaceous separation point suite, New Zealand, using U-Pb isotopes, REE and Ti geothermometry. *Contributions to Mineralogy Petrology*, 156(2): 133–160
- Bryant DL, Ayers JC, Gao S, Miller CF and Zhang H. 2004. Geochemical, age, and isotopic constraints on the location of the Sino-Korean-Yangtze suture and evolution of the northern Dabie complex, east central China. *Geological Society of America Bulletin*, 116(5–6): 698–717
- Burnham, AD and Berry AJ. 2012. An experimental study of trace element partitioning between zircon and melt as a function of oxygen fugacity. *Geochimica et Cosmochimica Acta*, 95: 196–212
- Chen FK, Guo JH, Jiang LL, Siebel W, Cong BL and Satir M. 2003. Provenance of the Beihuaiyang lower-grade metamorphic zone of the Dabie ultrahigh-pressure collisional orogen, China: Evidence from zircon ages. *Journal of Asian Earth Sciences*, 22(4): 343–352
- Dai LQ, Zhao ZF, Zheng YF, Li QL, Yang YH and Dai MN. 2011. Zircon Hf-O isotope evidence for crust-mantle interaction during continental deep subduction. *Earth and Planetary Science Letters*, 308(1): 229–244
- Duan C, Li YH, Hou KJ, Yuan SD, Liu JL and Zhang C. 2012. Late Mesozoic ore-forming events in the Ningwu ore district, middle-lower Yangtze River polymetallic ore belt, East China: Evidence from zircon U-Pb geochronology and Hf isotopic compositions of the granodioritic stocks. *Acta Geologica Sinica*, 86(3): 719–736
- Elhoul S, Belousova E, Griffin WL, Pearson NJ and O'Reilly SY. 2006. Trace element and isotopic composition of GJ-red zircon standard by laser ablation. *Geochimica et Cosmochimica Acta*, 70(18): A158
- Fan WM, Guo F, Wang YJ and Zhang M. 2004. Late Mesozoic volcanism in the northern Huaiyang tectono-magmatic belt, central China: Partial melts from a lithospheric mantle with subducted continental crust relicts beneath the Dabie orogen? *Chemical Geology*, 209(1–2): 27–48
- Gao S, Luo TC, Zhang BR, Zhang HF, Han YM, Zhao ZD and Hu YK. 1998a. Chemical composition of the continental crust as revealed by studies in East China. *Geochimica et Cosmochimica Acta*, 62(11): 1959–1975
- Gao S, Zhang BR, Jin ZM, Kern H, Zhao ZD and Luo TC. 1998b. How mafic is the lower continental crust? *Earth and Planetary Science Letters*, 161(1): 101–117
- Griffin WL, Pearson NJ, Belousova E, Jackson SE, Achterbergh EV, O'Reilly SY and Shee SR. 2000. The Hf isotope composition of cratonic mantle: LAM-MC-ICPMS analysis of zircon megacrysts in kimberlites. *Geochimica et Cosmochimica Acta*, 64(1): 133–147
- Hacker BR, Ratschbacher L, Webb L, Ireland T, Walker D and Dong SW. 1998. U-Pb zircon ages constrain the architecture of the ultrahigh-pressure Qinling-Dabie Orogen, China. *Earth and Planetary Science Letters*, 161(1–4): 215–230
- Hacker BR, Ratschbacher L, Webb LE, Ireland TR, Calvert A, Dong S, Wenk HR and Chateigner D. 2000. Exhumation of ultrahigh-pressure continental crust in east-central China: Late Triassic-Early Jurassic tectonic unroofing. *Journal of Geophysical Research*, 105(B6): 13339–13364
- Hacker BR, Ratschbacher L and Liu JG. 2004. Subduction, collision and exhumation in the ultrahigh-pressure Qinling-Dabie orogen. In: Malpas J, Fletcher C and Ali JR (eds.). *Aspects of the Tectonic Evolution of China*, Vol. 226. Geological Society, Special Publication, London, 157–175
- He YS, Li SG, Hoefs J, Huang F, Liu SA and Hou ZH. 2011. Post-collisional granitoids from the Dabie orogen: New evidence for partial melting of a thickened continental crust. *Geochimica et Cosmochimica Acta*, 75(13): 3815–3838
- He YS, Li SG, Hoefs J and Kleinhanns IC. 2013. Sr-Nd-Pb isotopic compositions of Early Cretaceous granitoids from the Dabie orogen: Constraints on the recycled lower continental crust. *Lithos*, 156–159: 204–217
- Hoskin PWO and Schaltegger U. 2003. The composition of zircon and igneous and metamorphic petrogenesis. *Reviews in Mineralogy and Geochemistry*, 53: 27–62
- Hou KJ, Li YH, Zou TR, Qu XM, Shi YR and Xie GQ. 2007. Laser ablation-MC-ICP-MS technique for Hf isotope microanalysis of zircon and its geological applications. *Acta Petrologica Sinica*, 23(10): 2595–2604 (in Chinese with English abstract)
- Huang F, Li SG, Dong F, Li QL, Chen FK, Wang Y and Yang W. 2007. Recycling of deeply subducted continental crust in the Dabie Mountains, central China. *Lithos*, 96(1–2): 151–169
- Huang F, Li SG, Dong F, He YS and Chen FK. 2008. High-Mg adakitic rocks in the Dabie orogen, central China: Implications for foundering mechanism of lower continental crust. *Chemical Geology*, 255(1–2): 1–13
- Huang F, Wang DH, Lu SM, Chen YC, Wang BH and Li C. 2011. Molybdenite Re-Os isotopic age of Shapinggou Mo deposit in Anhui Province and Mesozoic Mo ore-forming stages in East Qinling-Dabie Mountain region. *Mineral Deposits*, 30(6): 1039–1057 (in Chinese with English abstract)
- Jahn BM, Wu FY, Lo CH and Tsai CH. 1999. Crust-mantle interaction induced by deep subduction of the continental crust: Geochemical and Sr-Nd isotopic evidence from post-collisional mafic-ultramafic intrusions of the northern Dabie complex, central China. *Chemical Geology*, 157(1–2): 119–146
- Keppler H and Wyllie PJ. 1991. Partitioning of Cu, Sn, Mo, W, U, and Th between melt and aqueous fluid in systems halopogranite-H₂O-HCl and halogranite-H₂O-HF. *Contributions to Mineralogy and Petrology*, 109(2): 139–150
- Leech ML. 2001. Arrested orogenic development: Eclogitization, delamination, and tectonic collapse. *Earth and Planetary Science Letters*, 185(1–2): 149–159
- Li FL. 2011. Geological characteristics and metallogenic epoch of Qianechong large-size porphyry mo deposit at the northern foot of Dabie Mountains, He'nan Province. *Mineral Deposits*, 30(3): 457–468 (in Chinese with English abstract)
- Li HM, Ye HS, Wang DH, Chen YC, Qu WJ and Du AD. 2009. Re-Os dating of molybdenites from Zhaiwa Mo deposit in Xiong'er Mountain, western Henan Province, and its geological significance. *Mineral Deposits*, 28(2): 133–142 (in Chinese with English abstract)
- Li SG, Xiao YL, Liou DL, Chen YZ, Ge NJ, Zhang ZQ, Sun SS, Cong BL, Zhang RY, Hart SR and Wang SS. 1993. Collision of the North

- China and Yangtze blocks and formation of coesite-bearing eclogites-timing and processes. *Chemical Geology*, 109(1-4): 89-111
- Li SG, Huang F, Nie YH, Han WL, Long G, Li HM, Zhang SQ and Zhang ZH. 2001. Geochemical and geochronological constraints on the suture location between the North and South China blocks in the Dabie orogen, central China. *Physics and Chemistry of the Earth, Part A: Solid Earth and Geodesy*, 26(9-10): 655-672
- Li SG and Yang W. 2003. Decoupling of surface and subsurface sutures in the Dabie orogen and a continent-collisional lithospheric-wedging model; Sr-Nd-Pb isotopic evidences of Mesozoic igneous rocks in eastern China. *Chinese Science Bulletin*, 48(8): 831-838
- Li Y, Li N, Yang YF, Wang P, Mi M, Zhang J, Chen HJ and Chen YJ. 2013. Geological features and geodynamic settings of the Mo deposits in the northern segment of the Dabie Mountains. *Acta Petrologica Sinica*, 29(1): 95-106 (in Chinese with English abstract)
- Li YF, Mao JW, Hu HB, Guo BJ and Bai FJ. 2005. Geology, distribution, types and tectonic settings of Mesozoic molybdenum deposits in East Qinling area. *Mineral Deposits*, 24(3): 292-304 (in Chinese with English abstract)
- Liang HY, Campel HI, Allen C, Sun WD, Liu CQ, Yu HX, Xie YW and Zhang YQ. 2006. Zircon Ce^{4+}/Ce^{3+} ratios and ages for Yulong ore-bearing porphyries in eastern Tibet. *Mineralium Deposita*, 41(2): 152-159
- Liu FL and Xue HM. 2007. Review and prospect of SHRIMP U-Pb dating on zircons from Sulu-Dabie UHP metamorphic rocks. *Acta Petrologica Sinica*, 23(11): 2737-2756 (in Chinese with English abstract)
- Liu XC, Jahn BM, Liu DY, Dong SW and Li SZ. 2004. SHRIMP U-Pb zircon dating of a metagabbro and eclogites from western Dabieshan (Hong'an Block), China, and its tectonic implications. *Tectonophysics*, 394: 171-192
- Liu YC, Li SG, Xu ST, Jahn BM, Zheng YF, Zhang ZQ, Jiang LL, Chen GB and Wu WP. 2005. Geochemistry and geochronology of eclogites from the Northern Dabie Mountains, central China. *Journal of Asian Earth Sciences*, 25: 431-443
- Ludwig K. 2003. User's manual for Isoplot 3.00: A geochronological toolkit for Microsoft Excel. Berkeley Geochronology Center Special Publication, 4: 70
- Mao JW, Zhang ZH, Yu JJ and Niu BG. 2003. Geodynamic settings of Mesozoic large-scale mineralization in North China and adjacent areas: Implication from the highly precise dating of ore deposits. *Science China (Series D)* 46(8): 838-851
- Mao JW, Xie GQ, Zhang ZH, Li XF, Wang YT, Zhang CQ and Li YF. 2005. Mesozoic large scale metallogenic pulses in North China and corresponding geodynamic settings. *Acta Petrologica Sinica*, 21(1): 169-188 (in Chinese with English abstract)
- Mao JW, Xie GQ, Bierlein F, Qu WJ, Du AD, Ye HS, Pirajno F, Li HM, Guo BJ, Li YF and Yang ZQ. 2008. Tectonic implications from Re-Os dating of Mesozoic molybdenum deposits in the East Qinling-Dabie orogenic belt. *Geochimica et Cosmochimica Acta*, 72(18): 4607-4626
- Mao JW, Pirajno F, Xiang JF, Gao JJ, Ye HS, Li YF and Guo BJ. 2011a. Mesozoic molybdenum deposits in the East Qinling-Dabie Orogenic belt: Characteristics and tectonic settings. *Ore Geology Reviews*, 43(1): 264-293
- Mao JW, Pirajno F and Cook N. 2011b. Mesozoic metallogeny in East China and corresponding geodynamic settings: An introduction to the special issue. *Ore Geology Reviews*, 43(1): 1-7
- Mao JW, Xie GQ, Duan C, Pirajno F, Ishiyama D and Chen YC. 2011c. A tectono-genetic model for porphyry-skarn-stratabound Cu-Au-Mo-Fe and magnetite-apatite deposits along Middle-Lower Yangtze River Valley, eastern China. *Ore Geology Reviews*, 43(1): 294-314
- Mao JW, Cheng YB, Chen MH and Pirajno F. 2013. Major types and time-space distribution of Mesozoic ore deposits in South China and their geodynamic settings. *Mineralium Deposita*, 48(3): 267-294
- Nowell GM, Kempton PD, Noble SR, Fitton JG, Saunders AD, Mahoney JJ and Taylor RN. 1998. High precision Hf isotope measurements of MORB and OIB by thermal ionization mass spectrometry: Insights into the depleted mantle. *Chemical Geology*, 149(3-4): 211-233
- Patchett PJ, Kouvo O, Hedge CE and Tatsumoto M. 1981. Evolution of continental crust and mantle heterogeneity: Evidence from Hf isotopes. *Contributions to Mineralogy Petrology*, 78(3): 279-297
- Ratschbacher L, Hacker BR, Webb LE, McWilliams M, Ireland T, Dong SW, Calvert A, Chateigner D and Wenk HR. 2000. Exhumation of the ultrahigh-pressure continental crust in east central China: Cretaceous and Cenozoic unroofing and the Tan-Lu fault. *Journal of Geophysical Research*, 105(B6): 13303-13338
- Ratschbacher L, Hacker BR, Calvert A, Webb LE, Grimmer JC, McWilliams MO, Ireland T, Dong S and Hu J. 2003. Tectonics of the Qinling (Central China): Tectonostratigraphy, geochronology, and deformation history. *Tectonophysics*, 366(1-2): 1-53
- Rubatto D and Gebauer D. 2000. Use of cathodoluminescence for U-Pb zircon dating by IOM microprobe: Some examples from the western Alps. In: *Cathodoluminescence in Geoscience*. Heidelberg, Germany: Springer-Verlag, 373-400
- Scherer EE, Cameron KL and Blichert JT. 2000. Lu-Hf garnet geochronology: Closure temperature relative to the Sm-Nd system and the effects of trace mineral inclusions. *Geochimica et Cosmochimica Acta*, 64(19): 3413-3432
- Shinogara H, Kazahaya K and Lowenstern JB. 1995. Volatile transport in a convecting magma column: Implications for porphyry Mo mineralization. *Geology*, 23(12): 1091-1094
- Soderlund U, Patchett PJ, Vervoort JD and Isachsen CE. 2004. The ^{176}Lu decay constant determined by Lu-Hf and U-Pb isotope systematics of Precambrian mafic intrusions. *Earth and Planetary Science Letters*, 219(3-4): 311-324
- Sun JG, Zhang Y, Xing SW, Zhao KQ, Zhang ZJ, Bai LA, Ma YB and Liu YS. 2012. Genetic types, ore-forming age and geodynamic setting of endogenous molybdenum deposits in the eastern edge of Xing-Meng orogenic belt. *Acta Petrologica Sinica*, 28(4): 1317-1332 (in Chinese with English abstract)
- Sun SS and McDonough WF. 1989. Chemical and isotopic systematics of oceanic basalts: Implications for mantle composition and processes. In: *Saunders AD and Norry MJ (eds.). Magmatism in the Ocean Basins*. Geological Society, London, Special Publication, 42(1): 315-345
- Tacker RC and Candela PA. 1987. Partitioning of molybdenum between magnetite and melt: A preliminary experimental study of partitioning of ore metals between silicic magmas and crystalline phases. *Economic Geology*, 82(7): 1805-1826
- Trail D, Bruce Watson E and Tailby ND. 2012. Ce and Eu anomalies in zircon as proxies for the oxidation state of magmas. *Geochimica et Cosmochimica Acta*, 97: 70-87
- Vanderhaeghe O and Teyssier C. 2001. Partial melting and flow of orogens. *Tectonophysics*, 342(3-4): 451-472
- Wang Q, Zhao Z and Xiong X. 2000. The ascertainment of Late-Yanshanian A-type granite in Tongbai-Dabie Orogenic Belt. *Acta Petrologica et Mineralogica*, 19(4): 297-306 (in Chinese with English abstract)
- Wang Q, Wyman DA, Xu JF, Jian P, Zhao ZH, Li CF, Xu W, Ma JL and He B. 2007. Early Cretaceous adakitic granites in the Northern Dabie Complex, central China: Implications for partial melting and delamination of thickened lower crust. *Geochimica et Cosmochimica Acta*, 71(10): 2609-2636
- Wang T, Guo L, Zheng YD, Donskaya T, Gladkochub D, Zeng LS, Li JB, Wang YB and Mazukabzov A. 2012. Timing and processes of late Mesozoic mid-lower-crustal extension in continental NE Asia and implications for the tectonic setting of the destruction of the North China Craton: Mainly constrained by zircon U-Pb ages from metamorphic core complexes. *Lithos*, 154: 315-345
- Wang XM, Liou JG and Mao HK. 1989. Coesite-bearing eclogite from the Dabie Mountains in Central China. *Geology*, 17(12): 1085-1088
- Wang YJ, Fan WM, Peng TP, Zhang HF and Guo F. 2005. Nature of the Mesozoic lithospheric mantle and tectonic decoupling beneath the

- Dabie orogen, Central China: Evidence from $^{40}\text{Ar}/^{39}\text{Ar}$ Ar geochronology, elemental and Sr-Nd-Pb isotopic compositions of early Cretaceous mafic igneous rocks. *Chemical Geology*, 220(3-4): 165-189
- Wei GQ, Yao JM, Zhao TP, Sun YL, Li J, Yuan ZL and Qiao B. 2009. Discovery of ~1.9Ga Mo deposit in the East Qinling orogen: Molybdenite Re-Os ages of the Longmudian Mo deposit in the Henan Province. *Acta Petrologica Sinica*, 25(11): 2747-2751 (in Chinese with English abstract)
- Williams IS. 1998. U-Th-Pb geochronology by ion microprobe. In: McKibben MA, Shanks WC III and Ridley WI (eds.). *Applications of Microanalytical Techniques to Understanding Mineralizing Processes*. *Reviews in Economic Geology*, 7: 1-35
- Wu FY, Lin JQ, Simon A, Wilde SA, Zhang XO and Yang JH. 2005. Nature and significance of the Early Cretaceous giant igneous event in eastern China. *Earth Planetary Science Letters*, 233(1-2): 103-119
- Wu YB, Zheng YF, Zhang SB, Zhao ZF, Wu FY and Liu XM. 2007. Zircon U-Pb ages and Hf isotope compositions of migmatite from the North Dabie terrane in China: Constraints on partial melting. *Journal of Metamorphic Geology*, 25(9): 991-1009
- Xiang BW. 2009. Research on the structural thermochronology and deformation modeling for post-orogenic dome structures of the north Dabie. Ph. D. Dissertation. Hefei: Hefei University of Technology (in Chinese with English summary)
- Xie GQ, Mao JW, Li RL and Bierlein FP. 2008. Geochemistry and Nd-Sr isotopic studies of Late Mesozoic granitoids in the southeastern Hubei Province, Middle-Lower Yangtze River belt, eastern China: Petrogenesis and tectonic setting. *Lithos*, 104(1-4): 216-230
- Xie GQ, Mao JW and Zhao HJ. 2011. Zircon U-Pb geochronology and Hf isotopic constraints on petrogenesis of Late Mesozoic intrusions in the southeast Hubei Province, Middle-Lower Yangtze River belt (MLYRB), East China. *Lithos*, 125(1-2): 693-710
- Xie GQ, Mao JW, Zhao HJ, Duan C and Yao L. 2012. Zircon U-Pb and phlogopite $^{40}\text{Ar}/^{39}\text{Ar}$ age of the Chengchao and Jinshandian skarn Fe deposits, Southeast Hubei Province, Middle-Lower Yangtze River valley metallogenic belt, China. *Mineralium Deposita*, 47(6): 633-652
- Xie Z, Zheng YF, Yan J and Qian H. 2004. Source evolution relationship between A-type granites and mafic rocks from Shacun in Dabieshan. *Acta Petrologica Sinica*, 20(5): 1175-1184 (in Chinese with English abstract)
- Xin HB and Qu XM. 2008. Relative oxidation states of ore-bearing porphyries inferred from Ce(IV)/Ce(III) ratio in zircon: Application to the porphyry copper belt at Gangense, Tibet. *Acta Mineralogica Sinica*, 28(2): 152-160 (in Chinese with English abstract)
- Xiong Q, Zheng JP, Yu CM, Su YP, Tang HY and Zhang ZH. 2008. Zircon U-Pb age and Hf isotope of Quanyishang A-type granite in Yichang: Signification for the Yangtze continental cratonization in Paleoproterozoic. *Chinese Science Bulletin*, 54(3): 436-446
- Xu HJ, Ma CQ and Ye K. 2007. Early Cretaceous granitoids and their implications for the collapse of the Dabie orogen, eastern China: SHRIMP zircon U-Pb dating and geochemistry. *Chemical Geology*, 240(3-4): 238-259
- Xu HJ, Ma CQ, Zhang J and Ye K. 2013. Early Cretaceous low-Mg adakitic granites from the Dabie orogen, eastern China: Petrogenesis and implications for destruction of the over-thickened lower continental crust. *Gondwana Research*, 23(1): 190-207
- Xu ST, Su W and Liu YC. 2000. Discovery of the eclogite and its petrography in the northern Dabie Mountain. *Chinese Science Bulletin*, 45(3): 273-278
- Xu ST, Liu Y, Chen G, Roberto C, France R, He M and Liu H. 2003. New finding of micro-diamonds in eclogites from Dabie-Sulu region in central-eastern China. *Chinese Science Bulletin*, 48(10): 988-994
- Yang JH, Wu FY and Wilde SA. 2003. A review of the geodynamic setting of large-scale Late Mesozoic gold mineralization in the North China Craton: An association with lithospheric thinning. *Ore Geology Reviews*, 23(3-4): 125-152
- Yang MZ, Zeng JN, Qin YJ, Li FL and Wan SQ. 2010. LA-ICP-MS zircon U-Pb and molybdenite Re-Os dating for Qian'echong porphyry-type Mo deposit in northern Dabie, China, and its geological significance. *Geological Science and Technology Information*, 29(5): 35-45 (in Chinese with English abstract)
- Yang YF, Chen YJ, Li N, Mi M, Xu YL, Li FL and Wan SQ. 2013. Fluid inclusion and isotope geochemistry of the Qian'echong giant porphyry Mo deposit, Dabie Shan, China: A case of NaCl-poor, CO₂-rich fluid systems. *Journal of Geochemical Exploration*, 124: 1-13
- Ye HS, Mao JW, Li YF, Guo BJ, Zhang CQ, Liu J, Yan QR and Liu GY. 2006. SHRIMP zircon U-Pb and molybdenite Re-Os dating for the superlarge Donggou porphyry Mo deposit in East Qinling, China, and its geological implication. *Acta Geologica Sinica*, 80(7): 1078-1088 (in Chinese with English abstract)
- You ZD, Han YJ, Yang WR, Zhang ZM, Wei BZ and Liu R. 1996. The High-Pressure and Ultra High-Pressure Metamorphic Belt in the East Qinling and Dabie Mountains, China. Wuhan: China University of Geosciences Press, 1-150
- Yuan SD, Hou KJ and Liu M. 2010. Timing of mineralization and geodynamic framework of iron-oxid-apatite deposits in Ningwu Cretaceous basin in the Middle-Lower Reaches of the Yangtze River, China: Constraints from Ar-Ar dating on phlogopites. *Acta Petrologica Sinica*, 26(3): 797-808 (in Chinese with English abstract)
- Zhai MG. 2010. Tectonic evolution and metallogenesis of North China Craton. *Mineral Deposits*, 29(1): 24-36 (in Chinese with English abstract)
- Zhang GW, Zhang BR, Yuan XC and Xiao QH. 2001. Qinling Belt and Continental Dynamics. Beijing: Science Press, 1-729 (in Chinese)
- Zhang H, Gao S, Zhong Z, Zhang B, Zhang L and Hu S. 2002. Geochemical and Sr-Nd-Pb isotopic compositions of Cretaceous granitoids: Constraints on tectonic framework and crustal structure of the Dabieshan ultrahigh-pressure metamorphic belt, China. *Chemical Geology*, 186(3-4): 281-299
- Zhang SB, Zheng YF, Wu YB, Zhao ZF, Gao S and Wu FY. 2006. Zircon isotope evidence for $\geq 3.5\text{Ga}$ continental crust in the Yangtze craton of China. *Precambrian Research*, 146(1-2): 16-34
- Zheng JP, Griffin WL, O'Reilly SY, Zhang M, Pearson N and Pan YM. 2006. Widespread Archean basement beneath the Yangtze craton. *Geology*, 34(6): 417-420
- Zheng YF, Fu B, Gong B and Li L. 2003. Stable isotope geochemistry of ultrahigh pressure metamorphic rocks from the Dabie-Sulu orogen in China: Implications for geodynamics and fluid regime. *Earth-Science Reviews*, 62(1-2): 105-161
- Zheng YF, Zhou JB, Wu YB and Xie Z. 2005. Low-grade metamorphic rocks in the Dabie-Sulu orogenic belt: A passive-margin accretionary wedge deformed during continent subduction. *International Geology Review*, 47(8): 851-871
- Zheng YF and Zhang SB. 2007. Formation and evolution of Precambrian continental crust of southern China. *Chinese Science Bulletin*, 52(1): 1-10
- Zhao ZF, Zheng YF, Wei CS, Wu YB, Chen FK and Jahn BM. 2005. Zircon U-Pb age, element and C-O isotope geochemistry of post-collisional mafic-ultramafic rocks from the Dabie orogen in east-central China. *Lithos*, 83(1-2): 1-28
- Zhao ZF, Zheng YF, Wei CS and Wu YB. 2007. Post-collisional granitoids from the Dabie orogen in China: Zircon U-Pb age, element and O isotope evidence for recycling of subducted continental crust. *Lithos*, 93(3-4): 248-272
- Zhao ZF, Zheng YF, Wei CS, Chen FK, Liu XM and Wu FY. 2008. Zircon U-Pb ages, Hf and O isotopes constrain the crustal architecture of the ultrahigh-pressure Dabie orogen in China. *Chemical Geology*, 253(3-4): 222-242
- Zhao ZF and Zheng YF. 2009. Remelting of subducted continental

lithosphere: Petrogenesis of Mesozoic magmatic rocks in the Dabie-Sulu orogenic belt. *Science in China (Series D)*, 52(9): 1295-1318

Zhao ZF, Zheng YF, Wei CS and Wu FY. 2011. Origin of postcollisional magmatic rocks in the Dabie orogen: Implications for crust-mantle interaction and crustal architecture. *Lithos*, 126(1-2): 99-114

附中文参考文献

侯可军, 李延河, 邹天人, 曲晓明, 石玉若, 谢桂青. 2007. LA-MC-ICP-MS 锆石 Hf 同位素的分析方法及地质应用. *岩石学报*, 23(10): 2595-2604

黄凡, 王登红, 陆三明, 陈毓川, 王波华, 李超. 2011. 安徽省金寨县沙坪沟钼矿辉钼矿 Re-Os 年龄——兼论东秦岭-大别山中生代钼成矿作用期次划分. *矿床地质*, 30(6): 1039-1057

李法岭. 2011. 河南大别山北麓千鹅冲特大隐伏斑岩型钼矿床地质特征及成矿时代. *矿床地质*, 30(3): 457-468

李厚民, 叶会寿, 王登红, 陈毓川, 屈文俊, 杜安道. 2009. 豫西熊耳山寨凹钼矿床辉钼矿-钼-钨年龄及其地质意义. *矿床地质*, 28(2): 133-142

李毅, 李诺, 杨永飞, 王玘, 糜梅, 张静, 陈红瑾, 陈衍景. 2013. 大别山北麓钼矿床地质特征和地球动力学背景. *岩石学报*, 29(1): 95-106

李永峰, 毛景文, 胡华斌, 郭保健, 白凤军. 2005. 东秦岭钼矿类型、特征、成矿时代及其地球动力学背景. *矿床地质*, 22(3): 292-304

刘福来, 薛怀民. 2007. 苏鲁-大别超高压岩石中锆石 SHRIMP U-Pb 定年研究——综述和最新进展. *岩石学报*, 23(11): 2737-2756

毛景文, 谢桂青, 张作衡, 李晓峰, 王义天, 张长青, 李永峰. 2005. 中国北方中生代大规模成矿作用的期次及其地球动力学背景.

岩石学报, 21(1): 169-188

孙景贵, 张勇, 邢树文, 赵克强, 张增杰, 白令安, 马玉波, 刘勇胜.

2012. 兴蒙造山带东缘内生钼矿床的成因类型、成矿年代及成矿动力学背景. *岩石学报*, 28(4): 1317-1332

王强, 赵振华, 熊小林. 2000. 桐柏-大别造山带燕山晚期 A 型花岗岩的厘定. *岩石矿物学杂志*, 19(4): 297-306

魏庆国, 姚军明, 赵太平, 孙亚莉, 李晶, 原振雷, 乔波. 2009. 东秦岭发现 ~1.9Ga 钼矿床——河南龙门店钼矿床 Re-Os 定年. *岩石学报*, 25(11): 2747-2751

向必伟. 2009. 北大别造山后伸展过程构造热年代学与变形模拟研究. 博士学位论文. 合肥: 合肥工业大学, 1-117

谢智, 郑永飞, 闫峻, 钱卉. 2004. 大别山沙村中生代 A 型花岗岩和基性岩的源区演化关系. *岩石学报*, 20(5): 1175-1184

辛洪波, 曲晓明. 2008. 西藏冈底斯斑岩铜矿带含矿岩体的相对氧化状态: 来自锆石 Ce(IV)/Ce(III) 比值的约束. *矿物学报*, 28(2): 152-160

杨梅珍, 曾键年, 覃永军, 李法岭, 万守全. 2010. 大别山北缘千鹅冲斑岩型钼矿床锆石 U-Pb 和辉钼矿 Re-Os 年代学及其地质意义. *地质科技情报*, 29(5): 35-45

叶会寿, 毛景文, 李永峰, 郭保健, 张长青, 刘珺, 闫全人, 刘国印. 2006. 东秦岭东沟超大型斑岩型钼矿 SHRIMP 锆石 U-Pb 和辉钼矿 Re-Os 年龄及其地质意义. *地质学报*, 80(7): 1078-1088

袁顺达, 侯可军, 刘敏. 2010. 安徽宁芜地区铁氧化物-磷灰石矿床中金云母 Ar-Ar 定年及其地球动力学意义. *岩石学报*, 26(3): 797-808

翟明国. 2010. 华北克拉通的形成演化与成矿作用. *矿床地质*, 29(1): 24-36

张国伟, 张本仁, 袁学诚, 肖庆辉. 2001. 秦岭造山带与大陆动力学. 北京: 科学出版社, 1-729